

國立交通大學

電機與控制工程學系

碩士論文

即時無線瞌睡偵測腦機介面系統



Real-time Wireless Brain Computer Interface for
Drowsiness Detection

研究生：張哲睿

指導教授：林進燈 博士

中華民國 九十八 年 七 月

即時無線瞌睡偵測腦機介面系統

Real-time Wireless Brain Computer Interface for Drowsiness Detection

研 究 生：張哲睿

Student : Che-Jui Chang

指導教授：林進燈 博士

Advisor : Dr. Chin-Teng Lin



A Thesis

Submitted to Department of Electrical and Control Engineering
College of Electrical Engineering
National Chiao Tung University
in Partial Fulfillment of the Requirements
for the Degree of Master
in
Electrical and Control Engineering
July 2009
Hsinchu, Taiwan, Republic of China

中華民國 九十八 年 七 月

即時無線瞌睡偵測腦機介面系統

學生：張哲睿

指導教授：林進燈 博士

國立交通大學電機與控制工程研究所

摘要

近年來，交通意外是一個造成駕駛死亡的至關重要原因，其中駕駛者的精神狀況不佳所造成車禍意外佔了絕大多數比例，所以開車駕駛瞌睡監控問題是我們嘗試克服之處，試著以人為方式來減少車禍發生。近年來相關的開車監控研究主要著重在使用者影像辨識上，瞳孔辨識、眨眼辨識或是偵測司機擺頭頻率，但是，這些影像相關研究存在著先天上的缺點，使用者必須正對鏡頭才能得到好的量測結果；此外為了克服此點，其他學者引進了生理參數來做為開車即時瞌睡狀況的比較依據，如心電圖、眼電圖、肌電圖或腦波圖等，較影像辨識來得直接與精確，使用者可以不必受影像定位之問題影響，本論文即對於此生理參數中腦波參數做進一步的探討，並且設計一套無線可攜式的腦波擷取系統與數位訊號處理平台並且搭配非監督式分析演算法做即時瞌睡判斷，其優勢在於可移除掉不同人、不同次測量中個別跟環境差異性。本論文藉由虛擬實境模擬環境所記錄下開車偏移量來當作瞌睡程度的參考，並與所發展的非監督式分析法的相互比對關係來證明此演算法對瞌睡程度偵測的能效與可行性，最後實現在數位訊號處理平台上。經由實際測試，可以成功在駕駛者有睡意時，利用聲音警示提醒駕駛保持清醒，確保開車時的安全。

關鍵字：瞌睡監控、腦波圖、無線可攜式、腦波擷取系統、數位訊號處理平台、
虛擬實境模擬環境、開車偏移量、非監督式分析法

Real-time Wireless Brain Computer Interface for Drowsiness Detection

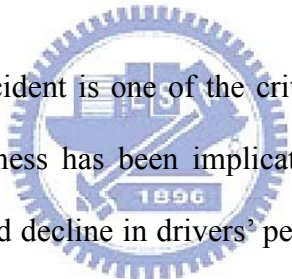
Student: Che-Jui Chang

Advisor: Dr. Chin-Teng Lin

Department of Electrical and Control Engineering

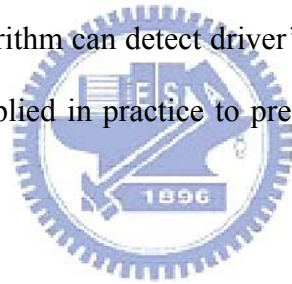
National Chiao Tung University

Abstract



In recent years, traffic accident is one of the critical reasons to cause deaths of drivers. Here, Drivers' drowsiness has been implicated as a causal factor in many accidents because of the marked decline in drivers' perception of risk and recognition of danger, and diminished vehicle handling abilities. Therefore, if the mental state of drivers can be real-time monitored directly, drowsiness detection and warning can effectively avoid disasters such as vehicle crashes in working environments. Some previous researches used non-physiological method, as eye closure with CCD image tracking, such as the pupil recognition, blink detection or identification the drivers head shaking frequency. However, for CCD image tracking, users couldn't move for free, and the images detecting performance were easily be interfered by light. And others used physiological parameters to increase the accuracy of drowsy detection, like pulse wave analysis with neural network, the electrooculogram (EOG) and the electromyography (EMG) measurement, and the electroencephalogram (EEG). In this study, we proposed a real-time wireless brain computer interface for drowsiness

detection. Here, a small, light, and portable EEG acquisition module was designed for long-time EEG monitoring. And a novel algorithm of drowsiness detection based on was also proposed to reduce the computation complexity, and was implemented in a portable DSP module. In order to estimate the level of drowsiness, a lane-keeping driving experiment was designed. The drowsiness level of drivers was indirectly assessed by the reaction time and driving trajectory under Virtual Reality Driving Simulation Environment. The advantage of this unsupervised algorithm can remove the differences between individual and environment in different people or measurements. In order to verify the accurate and feasibility of our proposed unsupervised algorithm, we compared drowsiness status estimated by driving performance with that obtained by our proposed unsupervised algorithm. The results showed that our proposed algorithm can detect driver's drowsiness status. Finally, our system can successfully be applied in practice to prevent traffic accidents caused by drowsy driving.



KEYWORD: drowsiness detection, electroencephalogram, portable EEG acquisition module, DSP module, Virtual Reality Driving Simulation Environment, driving performance, unsupervised algorithm

誌謝

本論文的完成，首先要感謝指導教授林進燈博士這兩年來的悉心指導，讓我學習到許多寶貴的知識，在學業及研究方法上也受益良多。另外也要感謝口試委員們的建議與指教，使得本論文更為完整。

其次，感謝實驗室的學長林伯昱、學長鍾仁峰及學長柯立偉在研究上的指導。同學有德、家欣、介恩、昕展，在過去兩年研究生活中同甘共苦、相互扶持，及學姐真如、依伶與毓婷、學長家達、孟修、煒忠、儀晟、寓鈞與建昇、學弟妹們育航、智賢、璽文、聖翔、佩瑄與佳鈴，在研究過程中所給我的鼓勵與協助，以及碩士班新生智綸、晉澤與琬茹在過去兩個月的幫忙。尤其是家達學長、依伶學姐及伯昱學長，在研究理論及程式技巧上給予我相當多的幫助與建議，亦師亦友，讓我獲益良多。也同樣感謝實驗室助理在許多事務上的幫助。

感謝我的父母親對我的教育與栽培，並給予我精神及物質上的一切支援，使我能安心地致力於學業，此外也感謝對我不斷的關心與鼓勵。最後我要感謝我的女朋友佳鈴，在我繁忙之中還有新鮮的水果可以享用，更不時叮嚀我的健康，有妳的陪伴讓我倍感窩心，使我能全心投入論文之中，謝謝你們。

謹以本論文獻給我的家人及所有關心我的師長與朋友們。

Contents

摘要.....	iii
Abstract.....	iv
誌謝.....	vi
Contents	vii
List of Tables.....	ix
List of Figures	x
Chapter1 Introduction	1
1.1 Brain Computer Interface	2
1.2 Previous Research.....	3
1.3 Motivation.....	8
1.4 Organization of Thesis	9
Chapter2 Material and Method	10
2.1 EEG Signal Acquisition	11
2.2 Virtual Reality Driving Simulation Environment.....	13
2.3 EEG Processing	16
2.4 Unsupervised Analysis.....	17
Chapter3 Hardware Framework.....	20
3.1 System Overview	20
3.2 Portable EEG Acquisition Module.....	21
3.2.1 Front-End Filter Circuit	22
3.2.2 Analog to Digital Converter.....	26
3.2.3 Digital Controller.....	27
3.2.4 Power Management	33
3.2.5 Wireless Transmission	34
3.3 DSP Module.....	35
3.3.1 DSP Framework.....	36
3.3.2 The Expanded SD Card Circuit	37
3.4 Hardware System Implementation.....	40
Chapter4 Unsupervised Approach	44
4.1 Driving Performance.....	44
4.2 Smoothing of the Power Spectra.....	47

4.3 Construction of the Alertness Model	48
4.4 Computation of the Deviation from the Subject	51
4.5 Driving Performance Sorting Analysis	52
Chapter5 Results and Discussion.....	54
5.1 Signal Test of Portable EEG Acquisition Module	54
5.1.1 Test for Sine Wave Signal	54
5.1.2 Test for Real EEG Signal	55
5.2 Driving Performance and Unsupervised Analysis	56
5.2.1 Results of Unsupervised Analysis.....	57
5.2.2 Relationship between Driving Performance and Unsupervised Analysis	60
5.2.3 Linear Combination of Model Deviations	61
5.2.4 Threshold Definition and Drowsiness Classification	62
5.2.5 DSP Module Programming.....	70
Chapter6 Conclusions	73
References.....	75



List of Tables

Table 2-1: Common band of EEG	12
Table 3-1: System specification of IA, HP, and LP filter for portable EEG acquisition module.....	25
Table 3-2: Definition and function for pins of SPI mode	29
Table 3-3: The spec of portable EEG acquisition module	42
Table 5-1: The comparison of the correlation between power and driving performance and MD* and driving performance for channel OZ	62
Table 5-2: The description of binary classification test	63
Table 5-3: The results of binary classification test	70



List of Figures

Fig. 1-1: The role of driver status monitor [48]	4
Fig. 1-2: Flowchart of EEG processing in drowsy estimation system [54]	6
Fig. 1-3: Flowchart of EEG processing in EEG-based drivers' cognitive states estimation system [55]	6
Fig. 1-4: Scan NuAmps Express system (Compumedics Ltd., VIC, Australia)	7
Fig. 2-1: A typical BCI system architecture	10
Fig. 2-2: International 10-20 system	13
Fig. 2-3: The overview of surrounded VR scene	14
Fig. 2-4: The digitized highway scene [61] ..	15
Fig. 2-5: Illustration of synchronization between the driving trajectory and EEG data	16
Fig. 2-6: Steps of EEG preprocessing	17
Fig. 2-7: Illustration of 8-second moving window with 7-second overlap	17
Fig. 2-8: The flowchart of the EEG analysis method	19
Fig. 3-1: Illustration of hardware framework of our BCI system	21
Fig. 3-2: Block diagram of Portable EEG acquisition module	22
Fig. 3-3: Circuits of preamplifier	23
Fig. 3-4: Simulation of preamplifier's gain response	23
Fig. 3-5: Circuits of band-pass filter	24
Fig. 3-6: Simulation of band-pass filter's gain response	24
Fig. 3-7: Simulation of gain response of the portable EEG acquisition module	25
Fig. 3-8: Handshake mode between AD7466 and MSP430F1611	26
Fig. 3-9: Functional block diagram of MSP430F1611	27
Fig. 3-10: Operating flow chart in MSP430F1611	28
Fig. 3-11: Timer_A up mode for interrupt function of MSP430F1611	29
Fig. 3-12: USART Master and external Slave	30
Fig. 3-13: Illustration for connection between four front-end circuits and digital control circuit	30
Fig. 3-14: Result of noise cancellation by using moving average	32
Fig. 3-15: Power supply circuit in portable EEG acquisition module	33
Fig. 3-16: Charging circuit in our portable EEG acquisition module	34
Fig. 3-17: PCB Blue Tooth antenna [77]	35
Fig. 3-18: The block diagram of DSP system	37
Fig. 3-19: Handshake mode between DSP module and expanded SD card circuit	37
Fig. 3-20: The function block diagram of MSP430F2013	38

Fig. 3-21: Schematic circuit of expanded SD card circuit.....	39
Fig. 3-22: Operating flow chart of expanded SD card circuit.....	40
Fig. 3-23: (a) The front-end analog circuit, (b) the digital control circuit, and (c) the whole portable EEG acquisition module with single channel.	41
Fig. 3-24: (a) The expanded SD card circuit and (b) illustration for application of expanded SD card circuit.....	43
Fig. 4-1: The example of deviation event and car trajectories.....	45
Fig. 4-2: The processing steps of driving performance	45
Fig. 4-3: Example of driving performance analysis. (a ~ d) are the fragment of information which marked by two lines.	46
Fig. 4-4: Processes of spectra analysis as precedence	48
Fig. 4-5: Process of sorting analysis	53
Fig. 5-1: The result of correlation between two conditions	55
Fig. 5-2: An example of alpha wave test. (a) shows EEG raw data, and (b) is the corresponding frequency domain spectra.	56
Fig. 5-3: Example 1 of driving performance and unsupervised analysis.....	58
Fig. 5-4: Example 2 of driving performance and unsupervised analysis.....	59
Fig. 5-5: The relationship between MDT / MDA and reaction time.....	61
Fig. 5-6: The relationship between sensitivity and specificity.....	63
Fig. 5-7: Positive predictive value vs. threshold of MD* (MDT, MTA, and MDC) ...	66
Fig. 5-8: Sensitivity vs. threshold of MD* (MDT, MTA, and MDC).....	67
Fig. 5-9: F-measure vs. threshold of MD* (MDT, MTA, and MDC).....	69
Fig. 5-10: The flowchart of DSP module program	70
Fig. 5-11: The user interface's flowchart	72
Fig. 5-12: The block diagram of dataflow	72

Chapter1 Introduction

In recent years, traffic accident is one of the critical reasons to cause deaths of drivers. World Health Organization report released that the global traffic accidents killed 1.2 million lives each year and caused millions of people were injured [1]. The report stated that a daily average of 1000 persons aged 25 years of age because of the people killed in traffic accidents, of which 90 percent of the victims took place mainly in Africa and Asia, low-income countries. The report said that the 19-year-old and 15-year-old groups to the cause of death, traffic accidents ranked first, far exceeding the number of AIDS deaths. It showed that the traffic safety is the very urgent issues that need to straighten and improve.

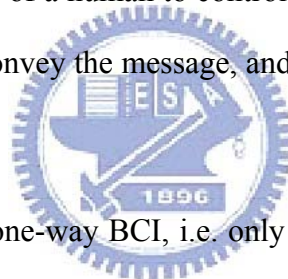
The cause of accidents is often imputed to driver's mental state. A human in drowsiness often exhibits relative inattention to environments, eye closure, less mobility, failure to motor control and decision making [2]. Therefore, those accidents which caused by falling drowsiness usually not only endanger themselves but also involve the public. Many studies have pointed out that a driver's drowsiness can cause serious traffic accidents [3]-[6]. In 2002, the National Highway Traffic Safety Administration (NHTSA) reported that about 0.7% of drivers have been involved in a crash that they attribute to drowsy driving, amounting to an estimated 800,000 to 1.88 million drivers in the past five years [7]. The National Sleep Foundation (NSF) also reported that 51% of adult drivers had driven a vehicle while feeling drowsy and 17% had actually fallen asleep [8].

Thus, in the field of safety driving, development of methodologies for detection drowsiness / departure from alertness in drivers has become an important area of researches. If the mental state of drivers can be real-time monitored directly,

drowsiness detection and warning can effectively avoid disasters such as vehicle crashes in working environments. Recently, with the development of brain computer interface, real-time monitoring the mental states of drivers and detecting drowsiness have become feasible.

1.1 Brain Computer Interface

Brain Computer Interface (BCI) is an interface between human and computers or machines. BCIs were aimed at assisting, augmenting or repairing human cognitive or sensory-motor functions. It is based on the translation of the specific brain activity generated by a specific thought of a human to control machines, to communicate with the outside world directly, to convey the message, and independent operations, as well as self-care purposes.



Current BCIs almost are one-way BCI, i.e. only external devices send signals to the brain [9], or receive commands from it [10]-[13], [14]-[41]. By acquisition of brain activities, BCI can be divided into three distinct modes: invasive, partially-invasive, and non-invasive BCI. Invasive BCI is implanted directly into the grey matter of the brain to obtain highest quality signals of brain activities or send external signals into the brain. But as the body reacts to a foreign object in the brain, scar-tissue is prone to buildup, and may cause the signals of BCI to become weaker or even lost. Partially invasive BCI is implanted inside the skull but rest outside the brain rather than among the grey matter. It produces better resolution signals than non-invasive BCI and has a lower risk of forming scar-tissue in the brain than invasive BCI. Electrocorticography (ECoG) is a typical technique used by partially-invasive BCI [10]-[13]. However, both invasive and partially-invasive BCIs

depend on surgical techniques. They are not friendly for general users.

Contrast to invasive and partially-invasive BCIs, non-invasive BCI is easy to wear, although non-invasive implants produce poor signal resolution due to that the skull dampens and blurs signals of brain activities. However, non-invasive BCI is still the main stream of BCI research. Non-invasive BCI has advantages of both easy application and absence of procedural risks, such as infection or cortical micro-lesions. There are several approaches to non-invasively acquire brain activities, such as magnetoencephalography (MEG), positron emission tomography (PET), functional magnetic resonance imaging (fMRI), electroencephalography (EEG) and et al. EEG is the mainstream of non-invasive BCI, because of its much fine temporal resolution, ease of use, portability and low set-up cost. In particular, higher temporal resolution becomes the great temptation to use EEG techniques as a direct communication channel from the brain to the real world [42], [43].



1.2 Previous Research

Drowsiness leads to decline in drivers' abilities of perception, recognition, and vehicle control and hence monitoring of drowsiness in drivers is very important to avoid road accidents [44]. Some researches used non-physiological method, as eye closure with CCD image tracking [45]-[51]. And others used physiological parameters to increase the accuracy of drowsy detection, like pulse wave analysis with neural network [55], the electrooculogram (EOG) and the electromyography (EMG) measurement [52], [53], and the electroencephalogram (EEG) [54]-[56].

In 2003, Hamada et al. proposed a driver status monitor system by using CCD camera, as shown in Fig. 1-1 [48]. The CCD camera was installed in the car and

focused on the user's eyes. The driver status monitor detected drowsiness from the change in the duration of eye closure during blinking and inattention from the change in the gaze direction. Using CCD camera to contribute the urgency system was a very difficult work here. There were some critical points inside, and needed to overcome. For instance, user couldn't move for free, the images detecting performance were easily be interfered by light, and the biggest problem was that the system is too big, complex, and expensive to implement. The algorithm of eye tracking also needed to use edge detecting to train data, and hence to build up a neural network to classify the drowsy status.

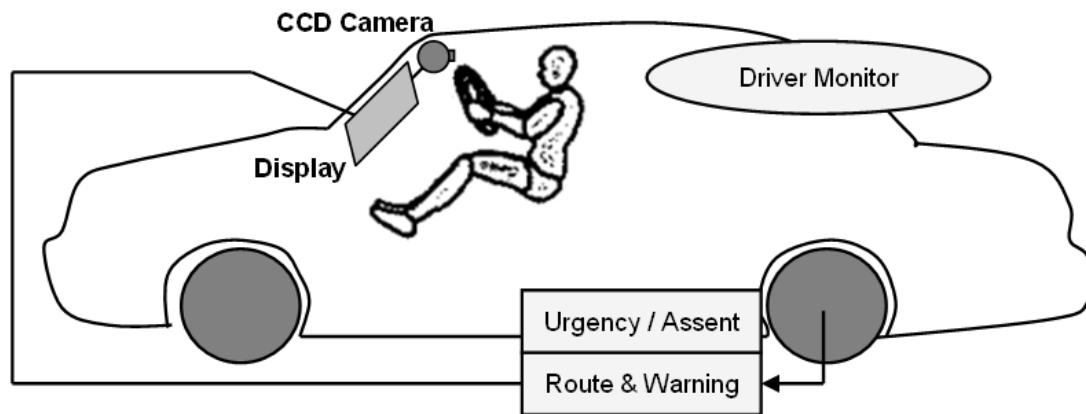


Fig. 1-1: The role of driver status monitor [48]

An alternate is to detect the moment from alertness to drowsiness by using physiological parameters. In 2005, Thum et al. used EOG as an alternative to video-based systems in detecting eye activities caused by drowsiness [53]. EOG is electrical signal generated by polarization of the eye ball and can be measured on skin around the eyes. Its magnitude varies in accordance to the displacement of the eye ball from its resting location. Rapid eye movements (REM), which occur when one is awake, and slow eye movements (SEM), which occur when one is drowsy, can be detected through EOG. The results showed that the detection rate for eye activities caused by drowsiness was more than 80 %.

In EEG system, it was different from other physiological parameters, and moreover it owned intuitive and specific characteristics, such as alpha, theta or beta band power followed subject's own mental state. In addition, the EEG system usually needed to collect enough EEG data to analyze. The supervised methods which previously study often had been used to train a learning data, and usually implement in off-line EEG analysis. Our previous studies which used supervised methods developed several kinds of brain computer interface for drowsiness detection [54], [55]. When the subject changed the state from alertness to drowsiness, the alpha rhythm will increase and beta rhythm will decrease [56]. In 2005, a drowsy estimation system was developed by combining independent component analysis (ICA), power-spectrum analysis, correlation evaluations, and linear regression model to estimate a driver's cognitive state when he/she drove a car in a virtual reality (VR)-based dynamic simulator [54]. Its flowchart of EEG processing was shown in Fig. 1-2. In 2006, an EEG-based drivers' cognitive states estimation system by using fuzzy neural network (FNN) was proposed [55]. Here, fuzzy neural network was used to train drowsiness estimation coefficients. The ICAFNN is a fuzzy neural network (FNN) capable of parameter self-adapting and structure self-constructing to acquire a small number of fuzzy rules for interpreting the embedded knowledge of a system from the given training dataset. Our experiments showed that the ICAFNN can achieve significant improvements in the accuracy of drowsiness estimation compared with our previous works. Its flowchart of EEG processing was shown in Fig. 1-3. In the above studies, an EEG machine, Scan NuAmps Express system (Compumedics Ltd., VIC, Australia), was used to measure EEG, as shown in Fig. 1-4. It is not small, light, and wearable. Moreover, the above algorithms for drowsiness detection requires mass computation complexity, thus, they are not easy to be implemented in a portable DSP device.

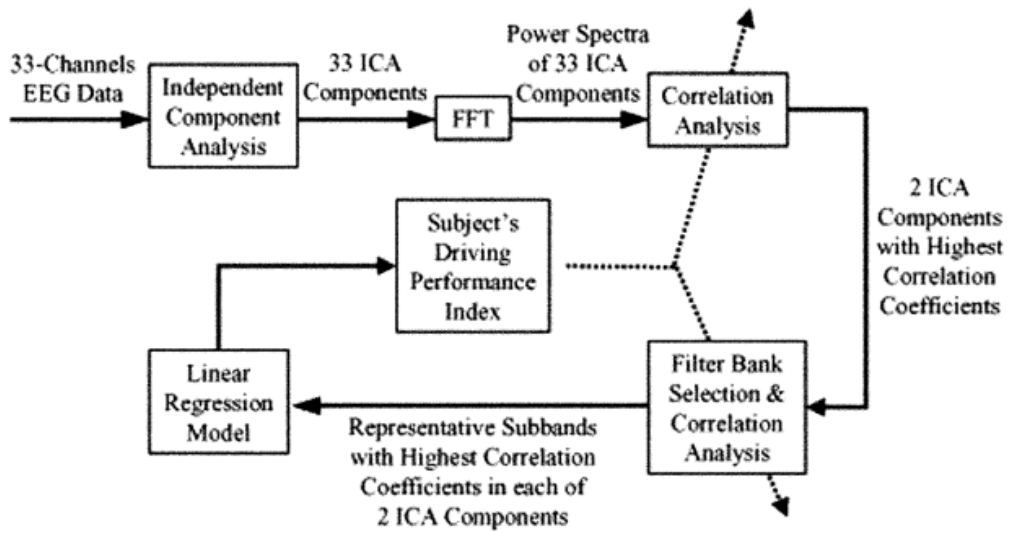


Fig. 1-2: Flowchart of EEG processing in drowsy estimation system [54]

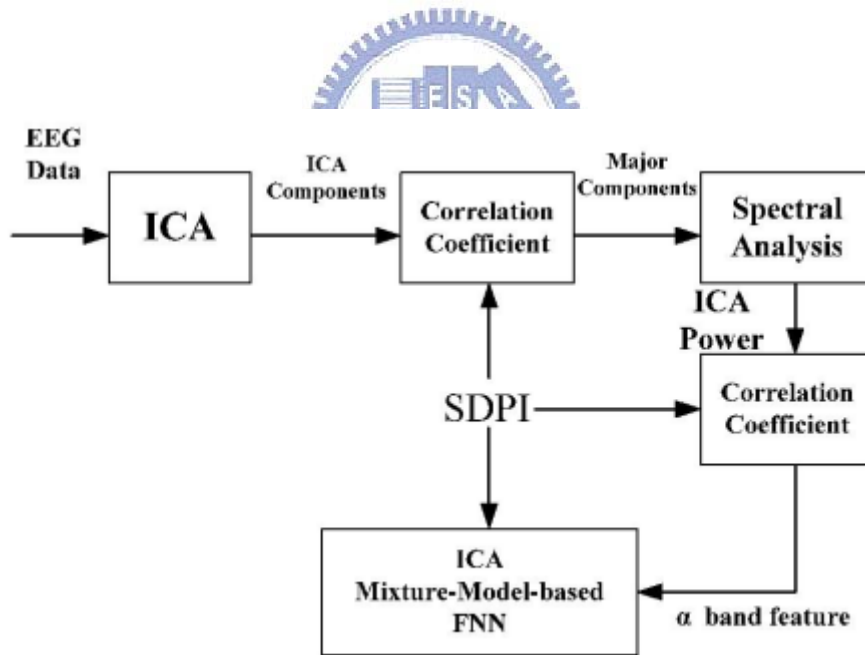


Fig. 1-3: Flowchart of EEG processing in EEG-based drivers' cognitive states estimation system [55]



Fig. 1-4: Scan NuAmps Express system (Compumedics Ltd., VIC, Australia)

In this mode, supervised learning methods such as artificial neural network (ANN) could be used to classify different states of vigilance. But stimulus may introduce some noise. So in [57], the author proposed a semi-supervised learning algorithm which can quickly label huge amount of data. Here another author proposed another kind of semi-supervised learning method based on probabilistic principle component analysis (PPCA) to distinguish wake, drowsy and sleep in driving simulation experiment. After training with data of around 20 min (6–8 min for each state), they could directly use our method as a real time classifier to estimate driver's vigilance state [58]. Although this method could greatly reduce the training time, but it still must used in off-line analysis. In our target, we wanted to find a non-training and unsupervised method, and easily implement to an on-line detecting system.

1.3 Motivation

Recently, the advance in sensor technology and information technology reduces the power consumption of the sensors and make the cost of production cheaper. These trends make it possible to embed sensors in different places or objects to measure a wide variety of physiological signals. A physiological signal monitoring system will be extremely useful in many areas if they are portable and capable of wirelessly monitoring target physiological signals and analyzing them in real time. However, the inconvenience of traditional BCI (heavy and large EEG machine) limits the user's mobility. Thus, portable and inexpensive BCI platform with long battery life that can be carried indoors or outdoors are desired.

In this study, we proposed a real-time wireless brain computer interface for drowsiness detection. Here, a small, light, and wearable EEG acquisition module was designed for long-time EEG monitoring. And a novel algorithm of drowsiness detection based on [59] was proposed to reduce the computation complexity. Different from previous ICA-based drowsiness detection algorithm, it used the statistics properties of alpha and theta rhythm in alert state to build up the alert model. Consequently, a derivation from the alert model can be used to detect drowsiness. The most useful advantage of this algorithm could remove the differences between individual and environment in different people or measurements, and every analysis were independent. Moreover, with the advantage of low computation complexity, it is easy to be implemented in a portable DSP module.

1.4 Organization of Thesis

In Chapter 2, it will describe that what is EEG signal, virtual reality driving simulation environment, and algorithms implemented in this thesis, which including EEG processing and unsupervised approach. In Chapter3, it will introduce how to implement a wireless portable EEG acquisition module and DSP module in hardware design. In Chapter 4, it will explain the detail of driving performance, unsupervised algorithm, and how to accomplish them. Finally, introduce the driving performance sorting analysis; then the method of driving performance and unsupervised approach will be verified with 15 real experimental subjects' driving trajectories and corresponding EEG signals, the procedures and results of verification will be described in Chapter 5. Finally it will have conclusion in Chapter 6.



Chapter2 Material and Method

We developed the BCI system according to the steps of Fig. 2-1. The portable EEG acquisition module which we designed was used in input device of BCI. The EEG raw data continually transmitted to DSP module, hence, the following three steps: signal processing, features extraction, and classifier, were processed in DSP module. The algorithm we chose was according to unsupervised approach (N. R. Pal, 2008 [59]). The user interface can output real-time EEG signal and the results of drowsy detection on the screen of DSP module. If the results were judged to drowsiness by algorithm, DSP module will call the buzzer to output a warning voice to wake user up as a BCI application.

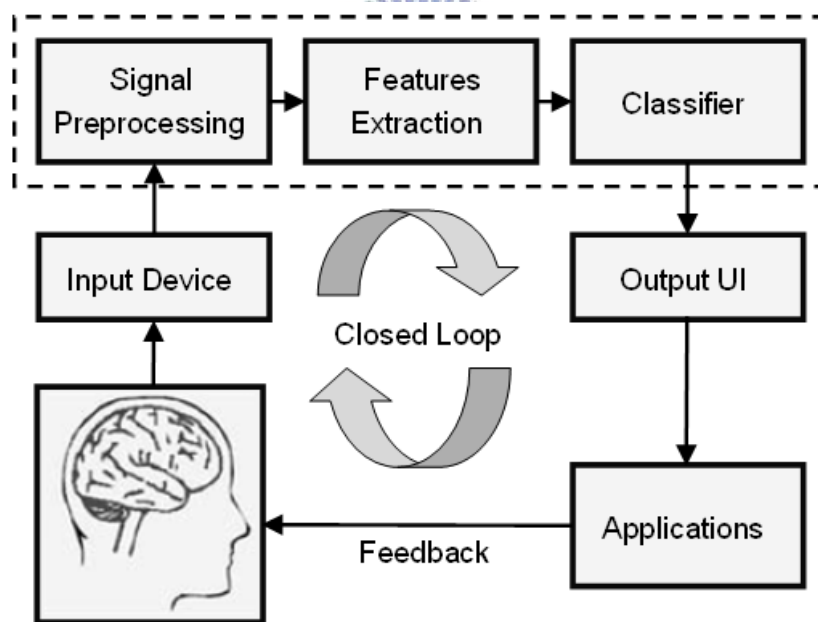
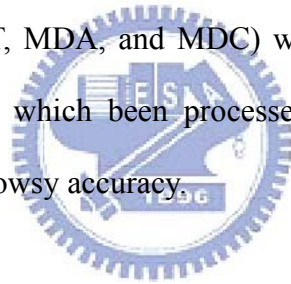


Fig. 2-1: A typical BCI system architecture

In off-line analysis, we wanted to verify the relationship between user's driving trajectories and corresponding EEG signal. Before analyzing, we assumed that driving trajectories were directly proportional with variance of theta and alpha spectrum. So we designed a driving simulation experiment and used our portable EEG acquisition

module to observe and record driving information and actual EEG raw data at one time. We recorded 15 subjects' EEG raw data and every one experimented 30 minutes. Our analysis included two parts: one was to analyze the driving trajectories, and another was to analyze the corresponding EEG signals. The first step of driving trajectories processing is to analyze the driving performance. On the other hand, we also analyze EEG signals. First, we use FFT to get the theta and alpha band information, and then using both two information built up an alert module, counting covariance matrix and mean vector of theta and alpha spectra. Furthermore, compute MDT, MDA, and MDC continually by using unsupervised method. After finishing both data analysis, we use binary classification test, sensitivity and specificity, to verify the drowsiness hit rate. Every experimental trial is separated and sorted, hence, the corresponding MD* (MDT, MDA, and MDC) will also be sorted. Defining the threshold of both information which been processed to decide the drowsiness or alertness, and to analyze the drowsy accuracy.



2.1 EEG Signal Acquisition

Electroencephalography (EEG) is the recording of electrical activity along the scalp produced by the firing of neurons within the brain. In clinical contexts, EEG refers to the recording of the brain's spontaneous electrical activity over a short period of time, usually 20–40 minutes, as recorded from multiple electrodes placed on the scalp [60]. When measuring from the scalps, recorded the EEG signal is about 10-100uV for a typical adult human. And a common system reference electrode is connected to the other input of each different amplifier. These amplifiers amplify the voltage between the active electrode and the reference (typically 1,000–100,000 times,

or 60–100 dB of voltage gain). The EEG is typically described in terms of rhythmic activity and transients. The rhythmic activity is divided into bands by frequency. The common band of EEG is shown as Table 2-1. Following the classification of EEG, Theta and Alpha band are related to drowsiness. Thus, when the subjects become drowsy, both bands will increase their power.

Table 2-1: Common band of EEG

Type	Frequency (Hz)	Normally
Delta	<4	Slow wave sleep for adults
Theta	4~7	Drowsiness, idling, or arousal in children and adults
Alpha	8~12	Relaxed, reflecting, or closing the eyes
Beta	12~30	Alert or working

There are high correlation between drowsiness and EEG obtained from the location of OZ in the international 10–20 EEG system [61]. Therefore, in this study, we only monitored EEG in the location of OZ. Here, three EEG electrodes were used. One is input, one is reference, and the other is ground. According to a modified International 10–20 EEG system and refer to right ear lobe as depicted in Fig. 2-2. We use the following notations: F: Frontal lobe. T: Temporal lobe. C: Central lobe. P: Parietal lobe. O: Occipital lobe. "Z" refers to an electrode placed on the mid-line. The input data is placed in OZ, ground is fixed in the center of forehead, and reference is pasted behind the right ear.

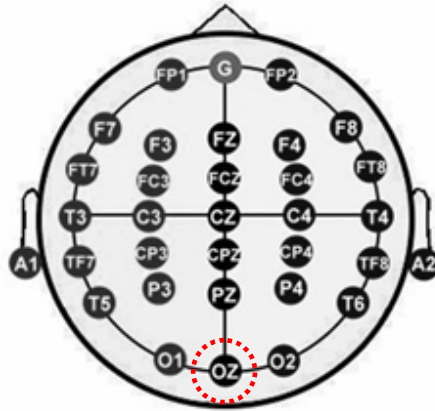


Fig. 2-2: International 10-20 system

Raw EEG data were recorded with 12-bit quantization level at the sampling rate of 512 Hz. To simplify the computation, raw EEG data were down-sampled to sampling rate of 64 Hz. And a simple moving average filter was used to remove 60 Hz power line noise and other high-frequency noise.



2.2 Virtual Reality Driving Simulation Environment

In this study, a lane-keeping driving experiment was utilized to investigate driving performance under different levels of drowsiness. Here, a virtual reality (VR)-based cruising environment was developed to simulate a car driving at 100 km/hr on a straight four-lane highway at night [54], [62]. During the driving experiments, all scenes move according to the displacement of the car and the subject's maneuvering of the wheels which make the subject feel like driving the car on a real road. The VR environment is showing in Fig. 2-3.



Fig. 2-3: The overview of surrounded VR scene. The VR-based highway scenes are projected into surround screen with seven projectors.

In all our experiments we have kept the driving speed fixed at 100 km/hr and system automatically and randomly drifts the car away from the center of the cruising lane to mimic the effects of a non ideal road surface. The driver is asked to maintain the car along the center of the cruising lane. All subjects involved in this study have good driving skill and hence when the subject is alert, his/her response time to the random drift is short and the deviation of the car from the center of the lane is small. But, when the subject is not alert / drowsy, both the response time and the car's deviation are high. Note that, in all our experiments, the subject's car is the only car cruising on the VR-based freeway. Although, both response time and the deviation from the central line are related to the subject's driving performance, in this study, we use the car's deviation from the central line as a measure of performance of the subjects. The driving task is showing in Fig. 2-4.

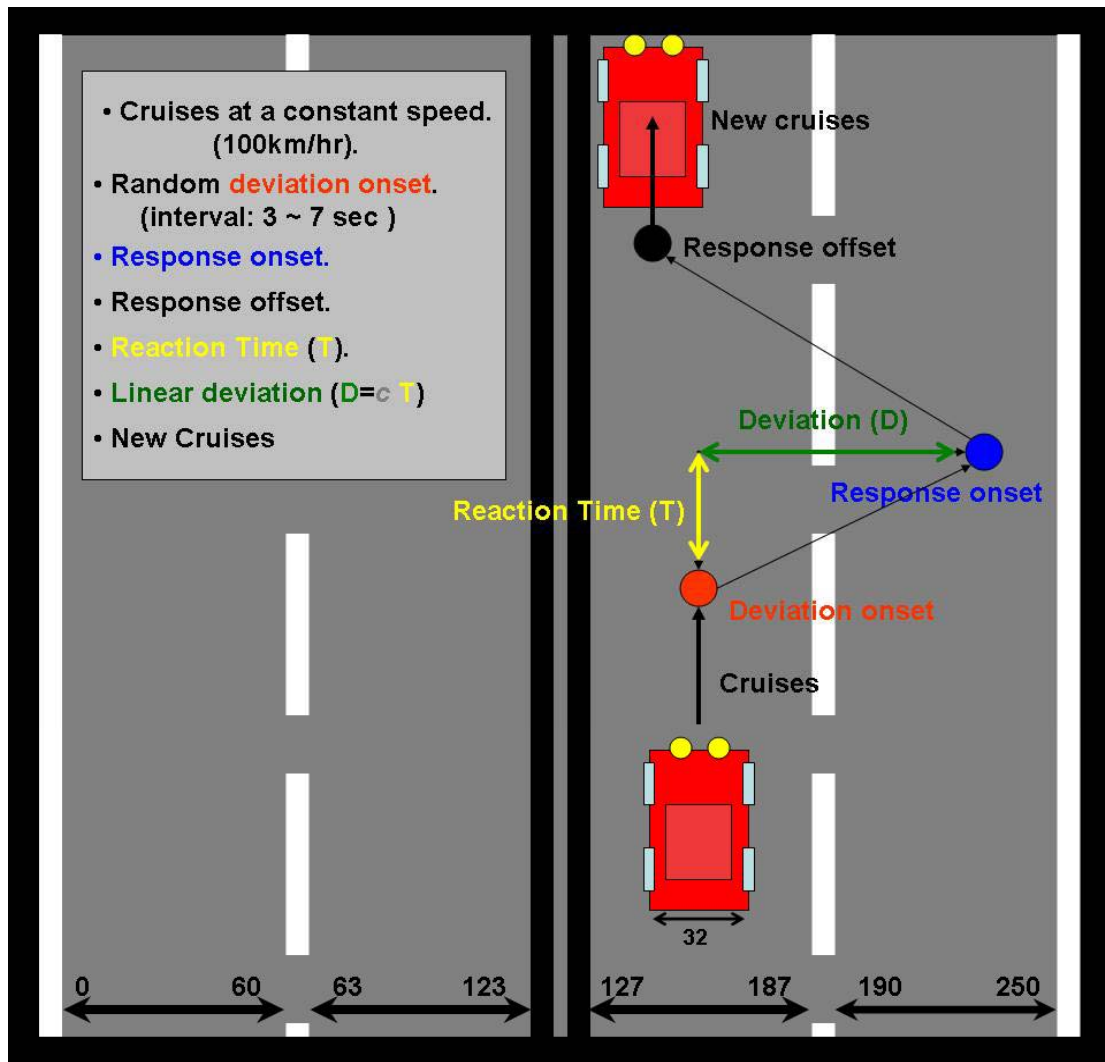


Fig. 2-4: The digitized highway scene. The width of highway is equally divided into 256 units and the width of the car is 32 units. An example of the deviation event. The car cruised with a fixed velocity of 100 km/hr on the VR-based highway scene and it was randomly drifted either to the left or to the right away from the cruising position with a constant velocity. The subjects were instructed to steer the vehicle back to the center of the cruising lane as quickly as possible [61].

In order to synchronize the records of driving trajectory and raw EEG data, a JAVA program was designed to record both of them at the same sampling rate. The driving trajectory produced from the VR-based cruising environment environment program, and raw EEG data obtained by portable EEG acquisition module were transmitted to JAVA program via RS232 and Blue tooth respectively. After finishing

the experiment, both the driving trajectory and raw EEG data were saved in a text file. Then, we can investigate the correlation between driving performance and results of unsupervised approach. The illustration of synchronization between the driving trajectory and EEG data was shown in Fig. 2-5.

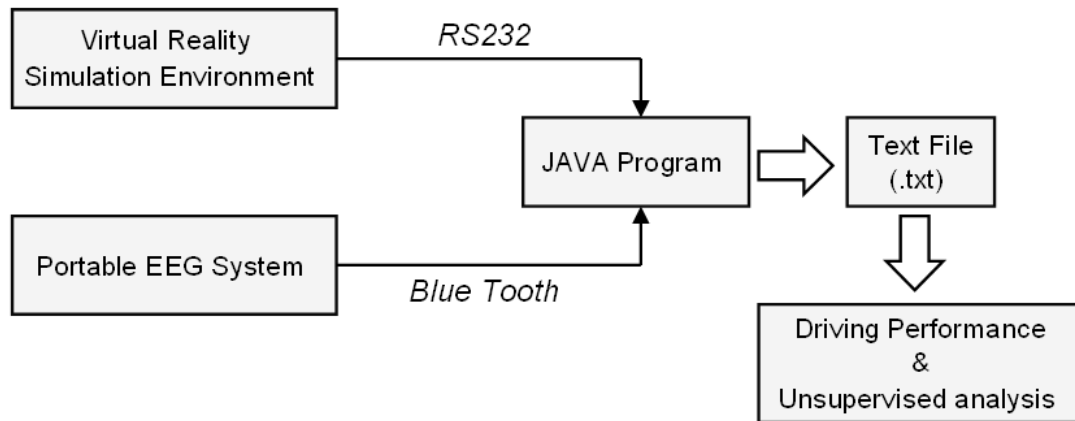


Fig. 2-5: Illustration of synchronization between the driving trajectory and EEG data



2.3 EEG Preprocessing

The EEG preprocessing steps were shown in Fig. 2-6. First, a simple moving average filter (low-pass filter with a cutoff frequency of 32 Hz) was used to remove 60 Hz power line noise and other high-frequency noise. In order to simplify the computation, raw EEG data were down-sampled to sampling rate of 64 Hz. Then, a 512-point moving window we designed to save the 8 seconds EEG information, as Fig. 2-7 shown. Finally, the power in the frequency band of alpha rhythm (8 ~ 11Hz) and theta rhythm (4 ~ 7Hz) was extracted.

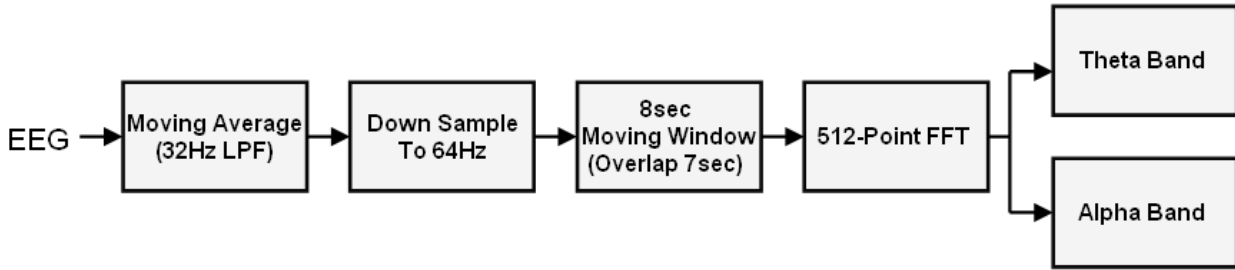


Fig. 2-6: Steps of EEG preprocessing

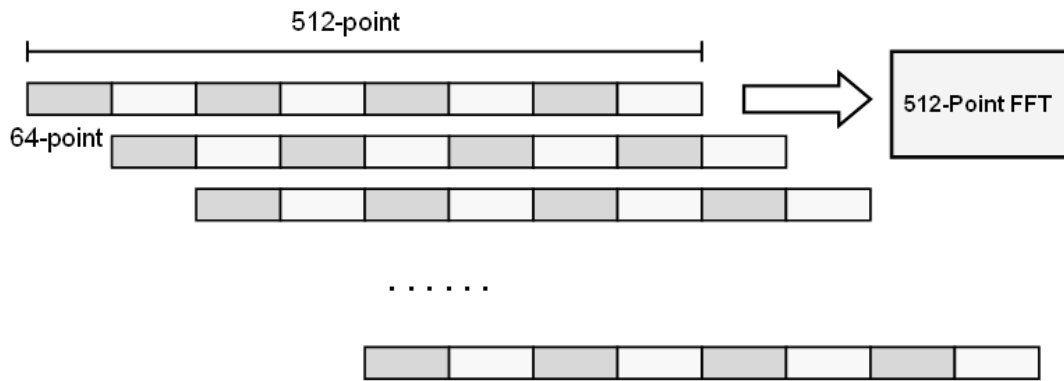


Fig. 2-7: Illustration of 8-second moving window with 7-second overlap

2.4 Unsupervised Analysis

It is recognized that the changes in EEG spectra in the theta band (4~7Hz) and alpha band (8~11Hz) reflect changes in the cognitive and memory performance [63]. Other studies have reported that EEG power spectra at the theta band [64], [65] and/or alpha band [66], [67] are associated with drowsiness, and EEG log power and subject's driving performance are largely linearly related.

As the above researches said, these findings have motivated us to derive the alert models of the driver using the alpha-band and theta-band EEG power spectrum computed using OZ channel output recorded in the first few minutes of driving. The

choice of the OZ channel is explained in the Experimental Results section. We emphasize that the few minutes of data used to find the alert model are not necessarily collected from the very beginning of driving session because different factors, such as walking of driver by a few meters to reach the garage, may influence the EEG signal generated at the very beginning. The specific window to be used for generation of the alert model is selected by Mardia test (explained later) [68]. We assume that if the subject/driver is in an alert state, then the EEG power spectra relating to theta band (as well as that relating to alpha band) would follow a multivariate normal distribution. The parameters of the multivariate normal distributions characterize the models. Using the alpha-band and theta-band EEG power, we identify two normal-distribution based models. Then, we assess the deviation of the current state of the subject from the alert model using Mahalanobis distance (MD). We assume that when the subject continues to remain alert, his/her EEG power should resemble the sample data used to generate the model and hence would match the alert model or template. If the subject becomes drowsy, then its power spectra in the alpha band (and also in theta band) will deviate from the respective model and hence MD will increase. With a view to reducing the effect of spurious noise, MDs are smoothed over a 90-sec moving windows, the window is moved by 1-sec steps [61]. We then study the relationship between smoothed Mahalanobis distance and subject's driving performance by computing the correlation between the two. Fig. 2-8 shows the overall flow of the EEG data analysis. In this figure, note that, after the models are identified, the preprocessed alpha band and theta band power data directly go to the blocks for computation of MDA and MDT, respectively. MDT and MDA are measure of deviations of the subject's present state from the respective models, this will be clarified later. The block for computation of MDC makes a linear combination of MDT and MDA. Finally, all three, MDA, MDT and MDC are used in correlation

analysis with the driver's performance.

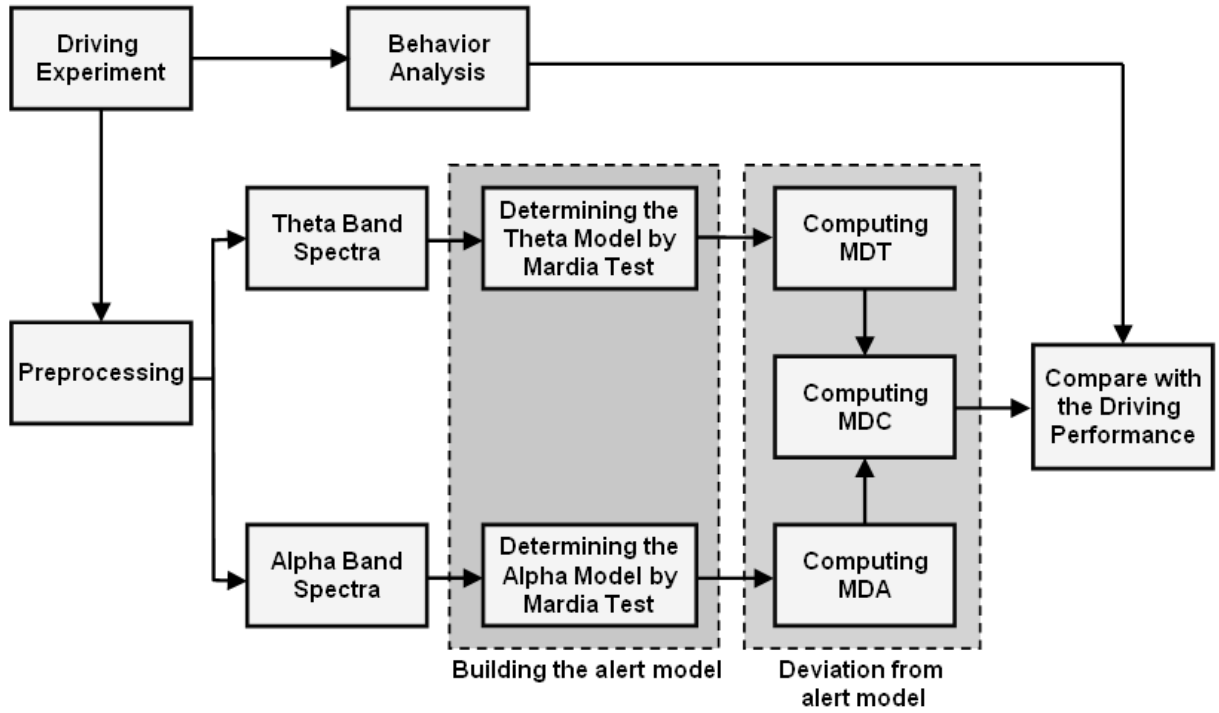


Fig. 2-8: The flowchart of the EEG analysis method.



Chapter3 Hardware Frameworks

In this chapter, we focus on this portable system hardware. Following the design flowchart, we will introduce the design methods of hardware circuits and firmware structures steps by steps.

3.1 System Overview

In order to online measure and analyze EEG signals, the whole hardware framework of our BCI mainly contains two sub-systems: One is portable EEG acquisition module, and the other is DSP module. First, EEG signal was measured by our portable EEG acquisition module continually. After amplifying tiny EEG signals, noise except the frequency band of EEG would be removed by filters in our portable EEG acquisition module. And then, filtered EEG signals would be digitized by analog-to-digital converter, and be transited to the DSP module via Bluetooth. Here, Linux kernel μ Clinux was used as the operation system in DSP module to handle user's applications. The major tasks of DSP module are to receive EEG signals via Bluetooth, and to execute the program of online drowsiness level detection, which monitor the variation of power of users' alpha rhythm and theta rhythm. The program of online drowsiness level detection would collect EEG data under alertness for first 3 minutes to build EEG alert model, and then calculated drowsiness level by assessing the power variation of alpha and theta rhythm every 2 seconds. If the power variation exceeded the threshold of alert model, the DSP module would send warning tone of buzzer to wake up users. The whole hardware framework is shown as Fig. 3-1.

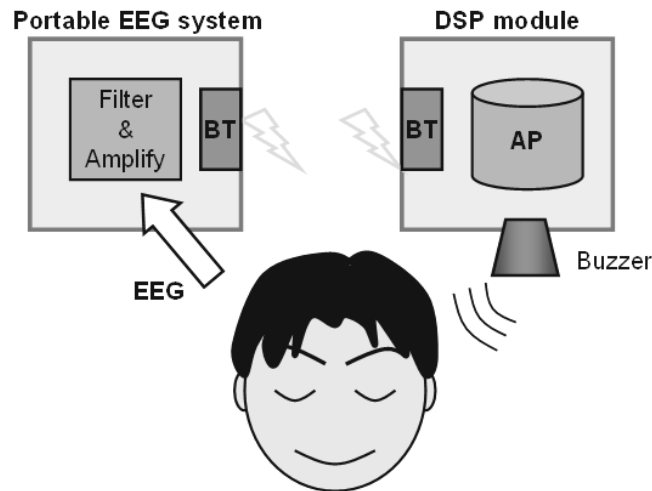


Fig. 3-1: Illustration of hardware framework of our BCI system

3.2 Portable EEG Acquisition Module

In order to be as small as possible and be easily wearable, a portable, distributive and wireless EEG headband system was designed to measure EEG signals. To reduce noise on PCB board produced by digital control circuit, the analog amplifier and digital control circuit were separated into two PCB boards. Following the previous researches [69], [70] worked, this general system was designed to minimize the circuit's size, use a simple microcontroller to handle programs, implement filter more accurate, and etc. We also referenced some circuit designs [71]-[76]. Those circuit designs followed portable and wireless rules, separating the circuit into client and server model. In this session, we interested in the client circuit design. The portable EEG acquisition module system mainly contains five parts: (1) front-end filter circuit, (2) analog to digital converter, (3) digital controller, (4) power management circuit and (5) wireless transmission. The system block diagram is shown in Fig. 3-2.

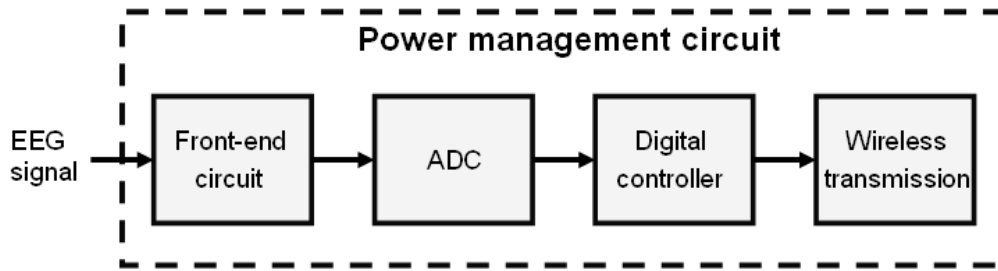


Fig. 3-2: Block diagram of Portable EEG acquisition module

3.2.1 Front-End Filter Circuit

The front-end circuit consisted of preamplifier, and band-pass filter. The total gain of front-end circuit was set as about 5040 times with the frequency band of 0.1~100 Hz. In some references, other circuit designs liked to use unit gain filters and one variable gain amplifier. Moreover, they didn't use a high-pass filter to cut-off the noise in low frequency band. To improve them, we designed a 3 stages high pass filter and 2 stages low pass filter to get the clear EEG information without noise. Hence, adding the gain into filter tried to minimize the total size.

A. Preamplifier

Here, instrumental amplifier LT1789-1 was used as the first stage of analog amplifier. LT1789-1 owns an ultra low input current and a high common-mode rejection ratio (CMRR) about 90dB. A high CMRR is important in applications that the signal of interest is represented by a small voltage fluctuation superimposed on a (possibly large) voltage offset, or when relevant information is contained in the voltage difference between two signals. Here, instrumental amplifier LT1789-1 provided not only the function of gain, but also that of one stage high pass filter by adding a capacitor. The corner frequency was set at 0.1Hz, and the gain was set to

2.25 times. The instrumental amplifier circuit was shown in Fig. 3-3, and the simulation of preamplifier's gain response was in Fig. 3-4.

$$gain = 1 + \frac{200k}{R_G} = 2.25 \quad f_0 = \frac{1}{2\pi * R1 * C1} = 0.099$$

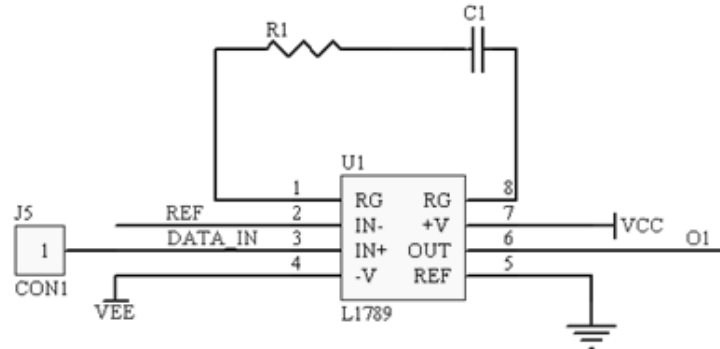


Fig. 3-3: Circuits of preamplifier

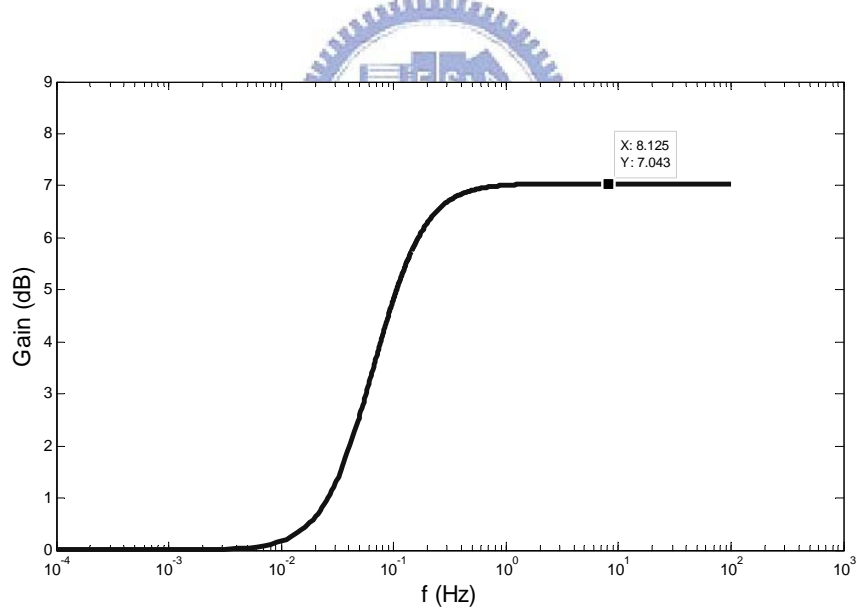


Fig. 3-4: Simulation of preamplifier's gain response

B. Band pass filter

In order to more precisely reserve relevant EEG signal, a band pass filter with frequency band of 0.1Hz ~ 100Hz and with gain of 1588.75 times was designed. The band-pass filter consisted of a 2nd-order high-pass filter and a 2nd-order low-pass

filter. Here, OP-AMP AD8607 was used to construct the band-pass filter. AD8607 also owns high CMRR (about 100dB), low input current, low distortion, and no phase reversal. The band-pass filter circuit was shown in Fig. 3-5, and the simulation of those gain response was in Fig. 3-6.

$$f_0 = \frac{1}{2\pi\sqrt{R2 * C2 * R4 * C3}} = 0.099 \quad (\text{High-pass corner frequency})$$

$$f_0 = \frac{1}{2\pi\sqrt{R8 * C4 * R9 * C5}} = 97.93 \quad (\text{Low-pass corner frequency})$$

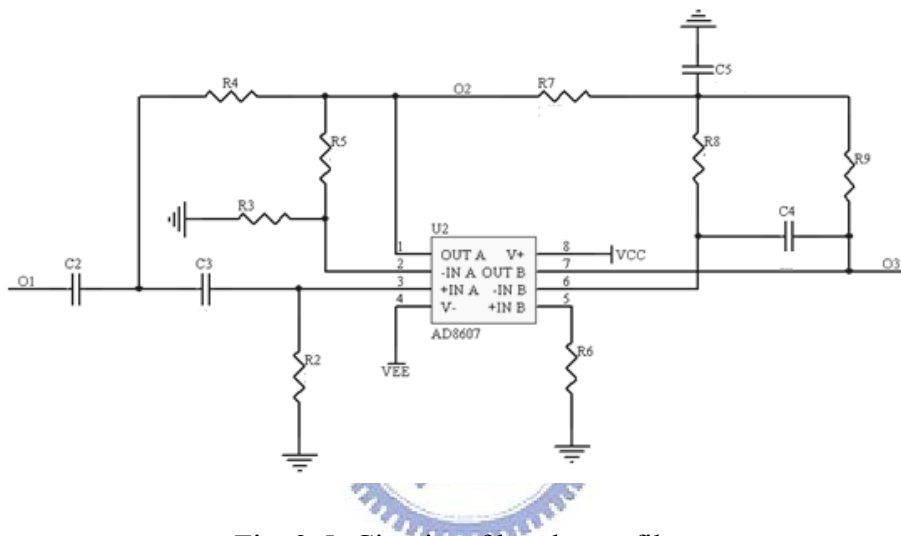


Fig. 3-5: Circuits of band-pass filter

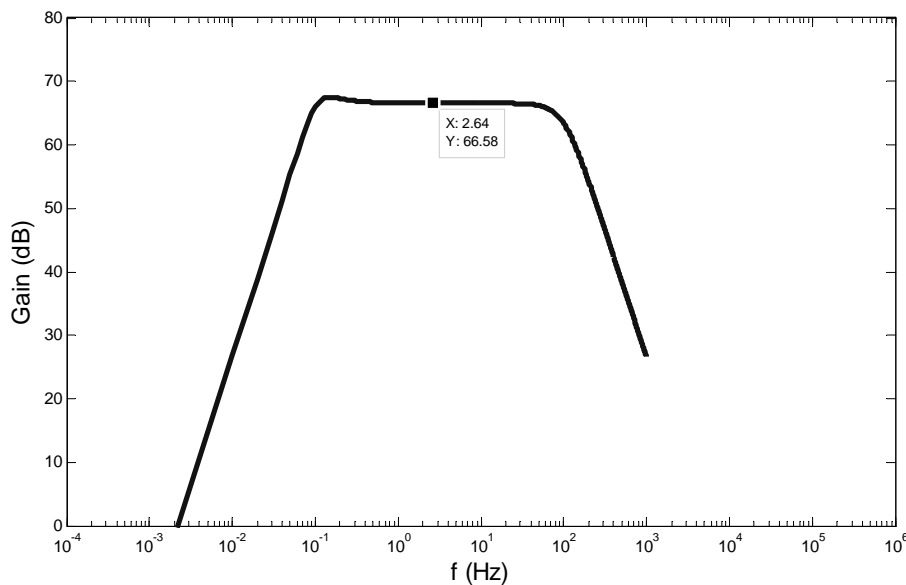


Fig. 3-6: Simulation of band-pass filter's gain response

The system specification of portable EEG acquisition module is listed below. The damping ratio of second order filter was set to 0.5, thus, the Bode diagram could be smoother in two sides of 3dB point as Table 3-1 described. The final simulation of gain response was shown in Fig. 3-7.

Table 3-1: System specification of IA, HP, and LP filter for portable EEG acquisition module

Orders	Type	Gain	Corner Freq.	Damping
Instrumental amplifier	Quasi HP	2.25	0.099	
High-pass filter	HP	43.7	0.099	0.5
Low-pass filter	LP	51.25	97.93	0.707

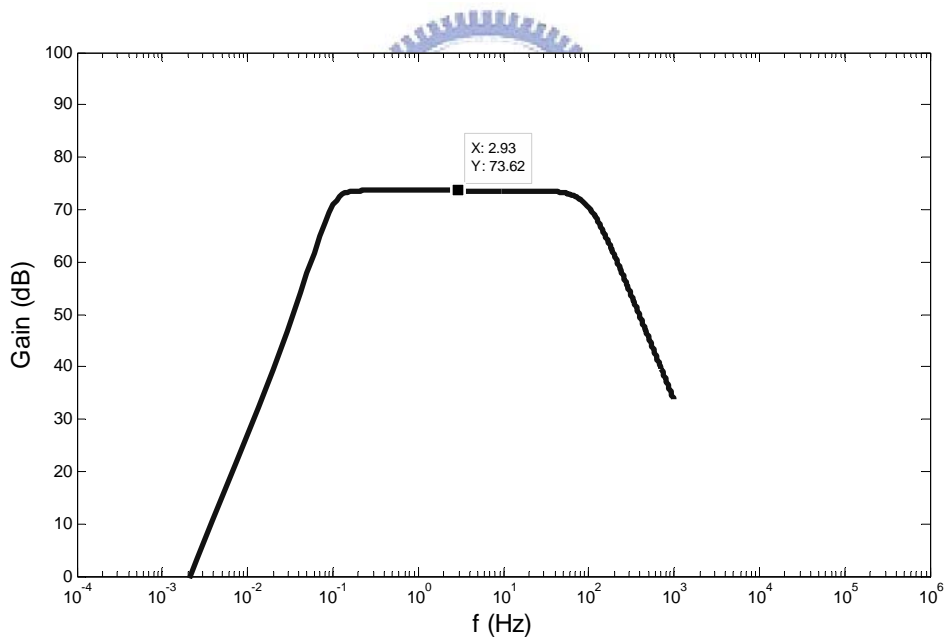


Fig. 3-7: Simulation of gain response of the portable EEG acquisition module

3.2.2 Analog to Digital Converter

The analog amplifier circuit and digital control circuit of our portable EEG acquisition module were placed individually in two PCB boards. There are some leading wires to connect both. A 12-bits analog-to-digital converter (ADC) AD7466 was used to convert continuous EEG signal of analog amplifier circuit to digitized EEG signal. Here, the micro-controller (MSP430F1611) was used to control ADC AD7466. The handshake mode between MSP430F1611 and AD7466 was shown in Fig. 3-8. The command signals and serial digitized EEG signal were transmitted via the serial peripheral interface (SPI) of MSP430F1611. The micro-controller MSP430F1611 outputs SCLK and CS signals in specific sampling rate 512Hz, and then digitized EEG signal would deliver into MSP430F1611. Each converting interval needed 16 cycles to complete transmission of digitized data, here, the data in first 4 cycles were zero, and the others were real 12-bit digitized data based on MSB.

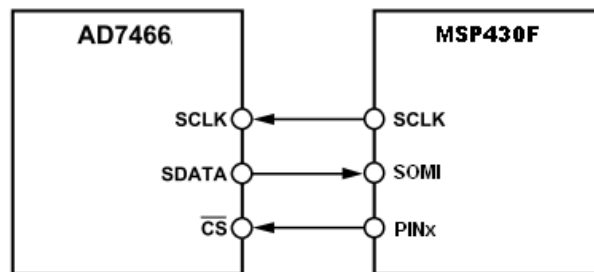


Fig. 3-8: Handshake mode between AD7466 and MSP430F1611

Moreover, according to equation (3-1), the conversion time is about $4.7 \mu\text{s}$, and 8-bit digitized data were transmitted every transmission cycle. And the maximum frequency of input signal of ADC was 100Hz. After calculating in equation (3-2) and (3-3), the result conforms to the equation (3-1). Thus, this system needn't a sample and hold amplifier to hold analog voltage.

$$\left(\frac{dV_{in}}{dt} \times t_a \right) \leq 1LSB \quad (3-1)$$

$$LSB = \frac{3V}{2^8} = 0.0117 \quad (3-2)$$

$$\left(\frac{dV_{in}}{dt} \times t_a \right) = \hat{V} \times 2\pi f \times t_a = 3 \times 2\pi \times 100 \times 4.7 \mu = 0.00886 \quad (3-3)$$

3.2.3 Digital Controller

The TI micro-controller MSP430F1611 was utilized to control other parts of circuits in portable EEG acquisition module. It owns many advantages for medical application, includes ultra-low power consumption, 16-bit RISC architecture, 125 ns instruction cycle time, five power saving modes, and diversification of peripheral communication interface. The functional block diagram of MSP430F1611 was shown in Fig. 3-9.

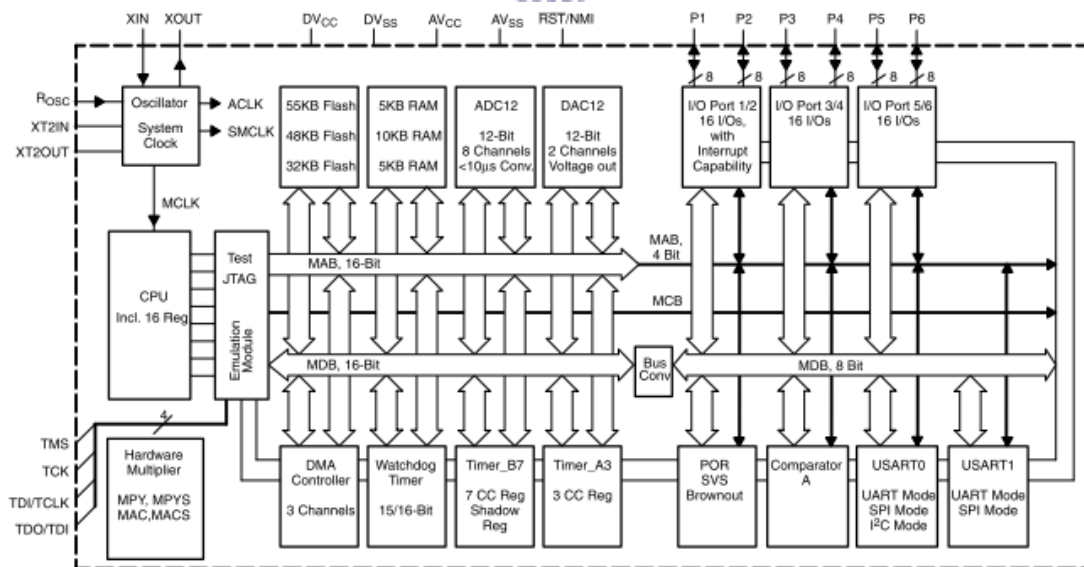


Fig. 3-9: Functional block diagram of MSP430F1611

MSP430F1611 catch digitized EEG signal from ADC AD7466 via serial

peripheral interface with sampling rate 512Hz, and then digitized EEG data were stored into memory of MSP430F1611. Next, a moving average filter was used to remove 60-Hz power line interference before wireless transmission. The operating flow chart in MSP430F1611 was shown in Fig. 3-10.

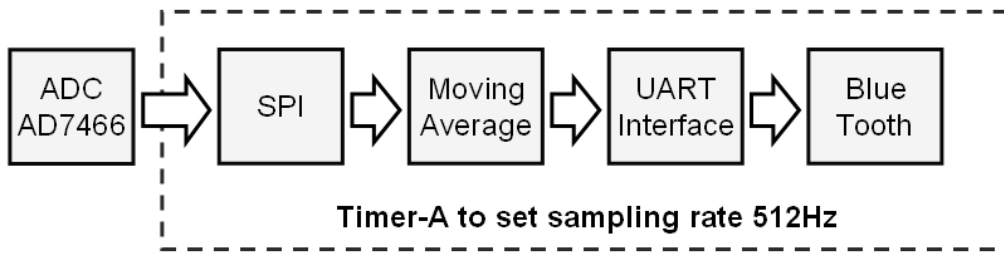


Fig. 3-10: Operating flow chart in MSP430F1611

A. Timer Interrupt

The interrupt function of MSP430F1611 is based on inner timer/counter register, called Timer_A, to count a specific time value. The counter value TACCR0 had to be set first, as shown in Fig. 3-11. When the timer counted to the TACCR0 value, the TACCR0 CCIFG interrupt flag would be set. And when the timer counted from TACCR0 to zero, the TAIFG interrupt flag would be set. In our portable EEG acquisition module, 4MHz crystal oscillator was used as system clock of MSP430F1611, and the sub-system master clock was set to 2MHz. Therefore, the operating cycle of program in MSP430F1611 would follow sub-system master clock. Thus, if the sampling rate of our EEG acquisition module is set to 512 Hz, TACCR0 has to be set to 3906.

$$TACCR0 = \frac{2M}{512} = 3906$$

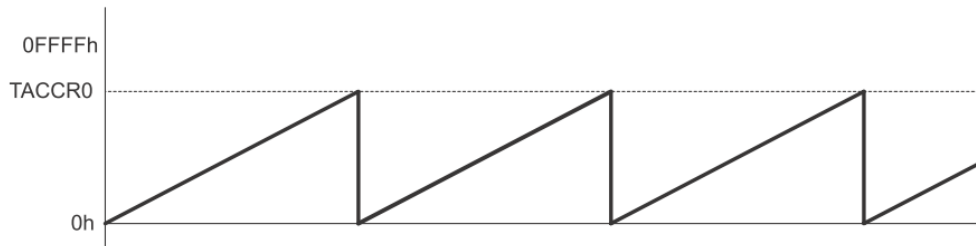


Fig. 3-11: Timer_A up mode for interrupt function of MSP430F1611

B. SPI Mode

In synchronous mode, the USART of MSP430F1611 connects to external systems via three or four pins: SIMO, SOMI, UCLK, and STE, as shown in Table 3-2.

Table 3-2: Definition and function for pins of SPI mode

SPI Mode	Operation
SIMO	Slave in, master out
SOMI	Slave out, master in
UCLK	USART SPI clock
STE	Slave transmit enable. Not used in 3-pin mode.

The master configuration of USART was shown in Fig. 3-12. The data transmission function of USART was initiated when transmitted data were moved to the transmit data buffer UxTXBUF. If the TX shift register was empty, then data in UxTXBUF would be moved into the TX shift register. When transmitted data were received, the received data were moved from the RX shift register to the received data buffer UxRXBUF and the receive interrupt flag URXIFGx would be set, that indicates the RX/TX operation was completed.

In our portable EEG acquisition module, the micro-controller MSP430F1611 can

cascade-connect with four front-end circuits via SPI, as shown in Fig. 3-13. Therefore, the handshake connection between Master module and Slave module needs 3-pin to transmit data: CS, SOMI, and UCLK. And there are four CS signal lines, one SOMI, and one UCLK signal line inside the leading wire.

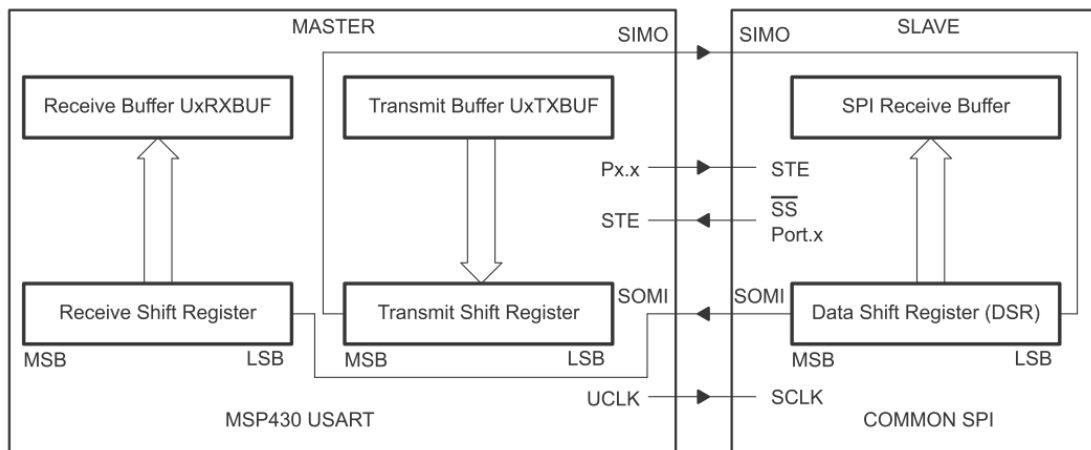


Fig. 3-12: USART Master and external Slave

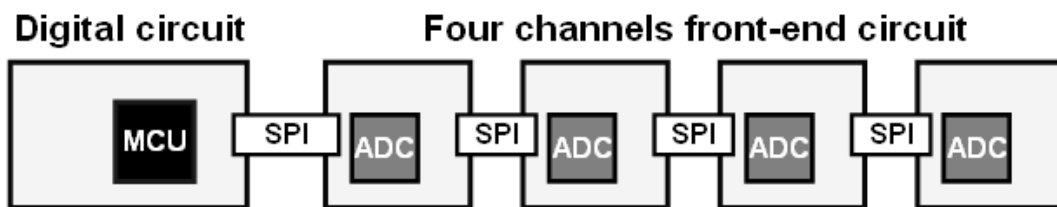


Fig. 3-13: Illustration for connection between four front-end circuits and digital control circuit

C. Moving Average

Moving average, also called rolling average or running average, is usually used to analyze a set of data points by creating a series of averages of different subsets of the full data set. Moving average can be applied to any data set, however, it is most commonly used with time series data to smooth out short-term fluctuations and highlight longer-term trends or cycles. The choice between short- and long- term, and

the setting of moving average parameters depends on the requirement of application. Mathematically, moving average is a type of convolution and is similar to a low-pass filter used in signal processing. The moving average filter is optimal for a common task: reducing random noise while retaining a sharp step response. This makes it as the premier filter for time domain encoded signals.

Given a sequence $\{a_i\}_{i=1}^N$, the output of an n -moving average is a new sequence $\{s_i\}_{i=1}^{N-n+1}$ defined as the average of subsequences of n terms. The formula of moving averaging was shown as followings.

$$s_i = \frac{1}{n} \sum_{j=1}^{i+n-1} a_j \quad (3-4)$$

Therefore, the sequences s_n of n -moving averages when $n = 2, 3$ can be expressed as

$$s_2 = \frac{1}{2}(a_1 + a_2, a_2 + a_3, \dots, a_{n-1} + a_n)$$

$$s_3 = \frac{1}{3}(a_1 + a_2 + a_3, a_2 + a_3 + a_4, \dots, a_{n-2} + a_{n-1} + a_n) \quad (3-5)$$

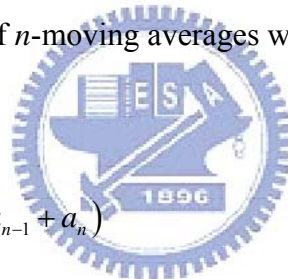


Fig. 3-14 shows the results of noise cancellation by using moving average. Here, a function generator was used to generate sin wave, and our portable EEG acquisition module was used to record this signal. If our portable EEG acquisition module was close to some electric instruments, the signal recorded from EEG acquisition module would easily be influenced by noise of 60 Hz power line. In the above figure of Fig. 3-14, it showed that the original sin wave had been contaminated by 60Hz power-line noise. After filtering by using moving average with 9-point moving window, we found moving average could effectively remove power-line noise, as shown in the below figure of Fig. 3-14.

$$Num_of_window = \frac{SampleRate}{60} = \frac{512}{60} = 8.53 \quad (3-6)$$

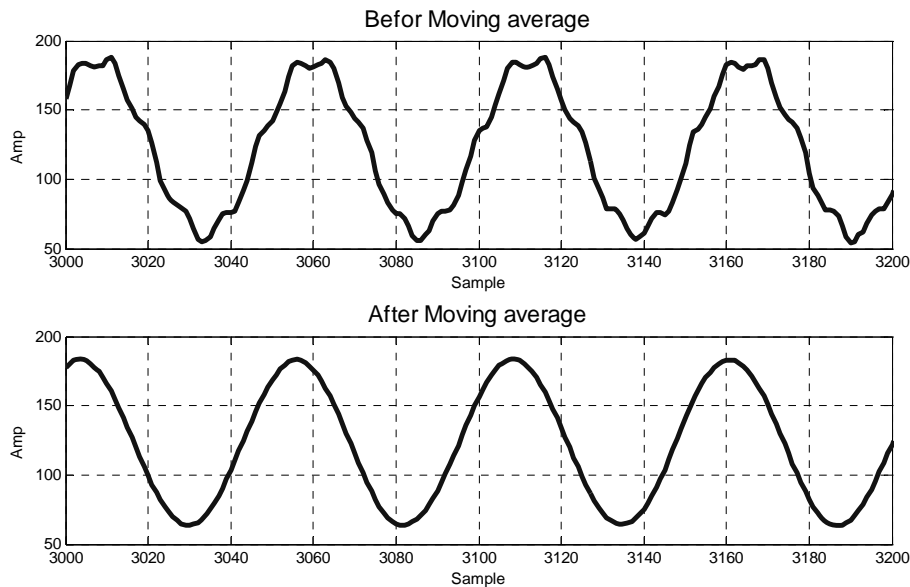


Fig. 3-14: Result of noise cancellation by using moving average

D. UART Interface

In asynchronous mode, USART connected MSP430 to external systems via two external pins, URXD and UTXD. In UART mode, USART transmitted and received characters at a bit rate asynchronously to another device. Timing for each character was based on the selected baud rate of USART. Here, the transmitter and receiver used the same baud rate. For initializing UART, RX and TX had to be enable first, and then decided the baud rate of UART and disable SWRST. The required division factor N for determining baud rate was listed as followings:

$$N = \frac{BRCLK}{\text{baud rate}} \quad (3-7)$$

Here, BRCLK was 4 MHz, and baud rate was 115200 bit/s. After initializing UART, the micro-controller could transmit data filtered by moving average to BLUE TOOTH module via UART.

3.2.4 Power Management

Power Management circuit in our portable EEG acquisition module includes two parts: one is power supply circuit, and the other is charging circuit.

A. Power Supply Circuit

In our portable EEG acquisition module, the operating voltage VCC was at 3V, and the virtual ground of analog circuit was at 1.5V. In order to provide stable 1.5V and 3V voltage, a regulator LP3985 was used to regulate battery voltage to 3V. Here, LP3985 is a micro-power, 150mA low noise, and ultra low dropout CMOS voltage regulator. The maximum output current can support 550mA. Furthermore, the turn-on time can reach 200 μ s. And a voltage divider circuit was used to divide 3V voltage into 1.5V, and a unity amplifier constructed from AD8628 was used to provide a voltage buffer. The total power supply circuit was shown in Fig. 3-15.

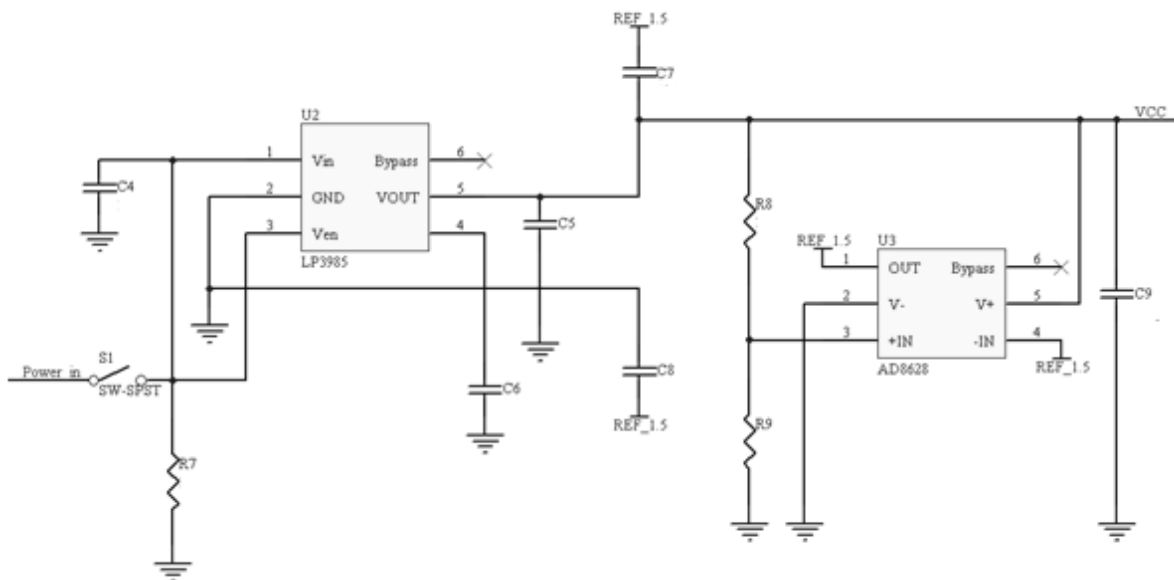


Fig. 3-15: Power supply circuit in portable EEG acquisition module

B. Charging Circuit

The charging circuit BQ24010DRC had integrated power FET and current sensor for 1-A charging applications. The maximum charging current can arrive to 1A. The battery's power would be detected automatically by charging circuit and switched to charging mode when battery's power was not enough. BQ24010DRC also protected battery to avoid over charging or over driving [77]. The charging circuit was shown in Fig. 3-16.

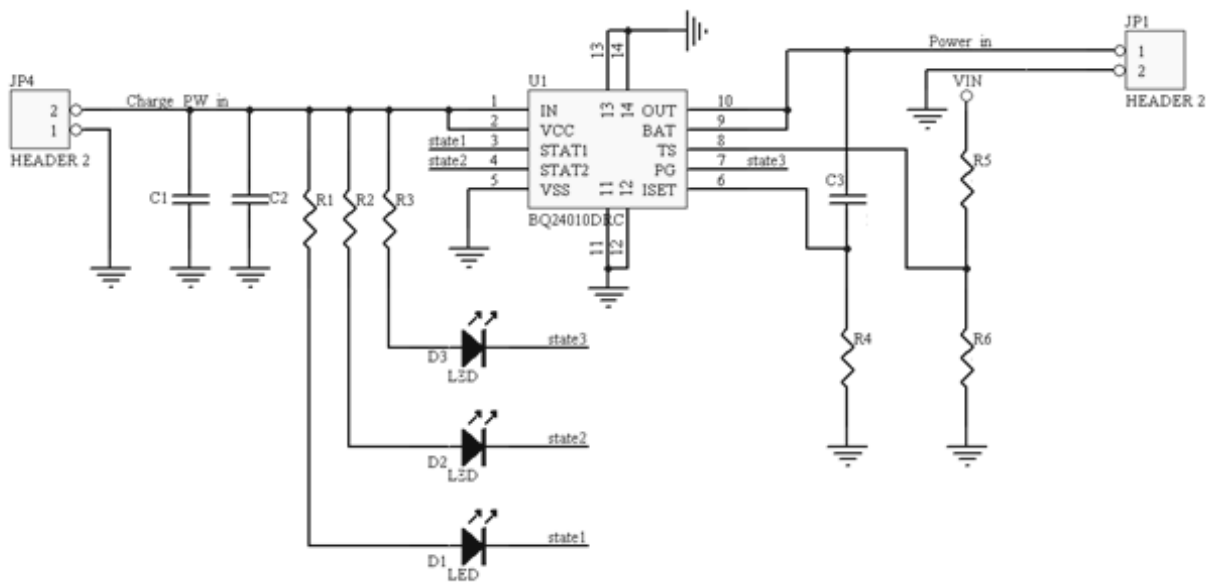


Fig. 3-16: Charging circuit in our portable EEG acquisition module

3.2.5 Wireless Transmission

Bluetooth is a wireless protocol utilizing short-range communication technology to facilitate data transmission over short distances from fixed and/or mobile devices. The intent behind the development of Bluetooth was the creation of a single digital wireless protocol, capable of connecting multiple devices and overcoming issues arising from synchronization of these devices. In this study, Bluetooth module

BM0203 was used. BM0203 is an integrated Bluetooth module to ease the design gap and uses CSR BlueCore4-External as the major Bluetooth chip. CSR BlueCore4-External is a single chip radio and baseband IC for Bluetooth 2.4GHz systems including enhanced data rates (EDR) to 3Mbps. It interfaces to 8Mbit of external Flash memory. When used with the CSR Bluetooth software stack, it provides a fully compliant Bluetooth system to v2.0 of the specification for data and voice communications. All hardware and device firmware of BM0203 is fully compliant with the Bluetooth v2.0 + EDR specification. Bluetooth operates at high frequency band to transmit wireless data, so it can be perfect worked by using a PCB antenna, as shown in Fig. 3-17.

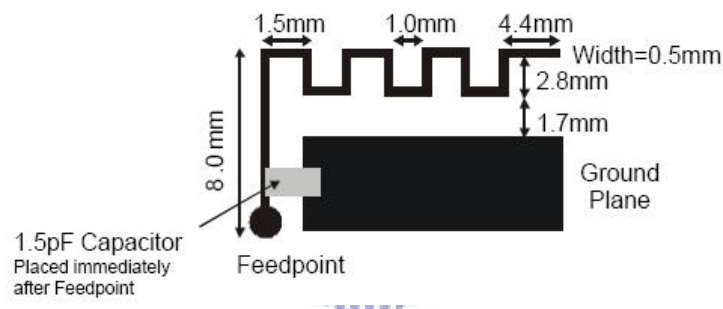


Fig. 3-17: PCB Blue Tooth antenna [77]

3.3 DSP Module

The design goal of DSP module is to build a back-end analysis platform. This platform not only has greatly powerful calculating ability, but also supports various peripheral interfaces. After measuring and pre-processing EEG signal by our portable EEG acquisition module, EEG signal would be transmitted to this DSP module via Bluetooth module. DSP module would then process and analyze EEG signal, and display results of EEG analysis on TFT LCD. Furthermore, it also can use other

peripheral interfaces to implement other applications [77].

3.3.1 DSP Framework

A powerful digital signal processor Analog Device BF533-STAMP was used in this DSP module, and its CPU speed can be up to 600MHz. It owns two 16-bit MAC, Multiply-And-Accumulate, to execute 1200 lines addition and multiplication functions. By the way, DSP contains many independent DMA, Direct Memory Access, to effectively reduce the processing time of core. The system block diagram was shown in Fig. 3-18. Here, Bluetooth module and UART both worked in the same UART interface.

TFT-LCD, worked by using Memory Mapping, shared the same Memory Bus with SDRAM. In order to reduce the size of platform, we decided to replace traditional parallel NOR Flash with SPI Flash, and it also shared with SD/MMC Socket. Furthermore, the DSP module also owned power management and charging circuits. SD/MMC Socket provided the interface scalability, such as SD/MMC Card, Sensor, ADC, Wireless Card, etc. In our application for drowsiness detection and warning, an expanded SD card circuit which can plug in SD card socket of DSP module was designed to produce buzzer. This circuit will be introduced in next session.

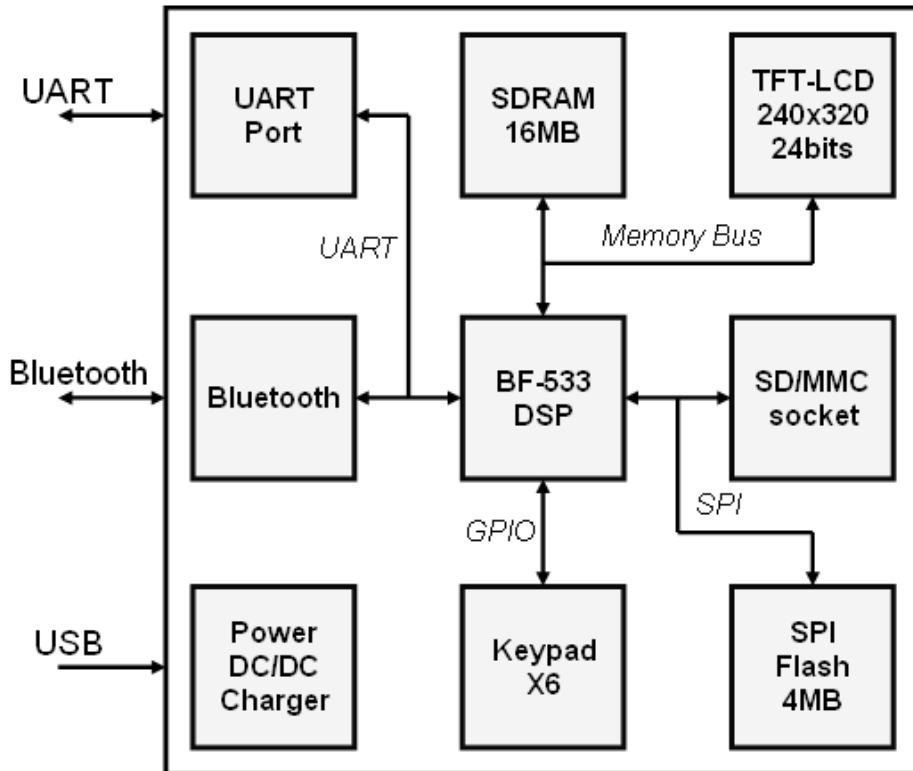
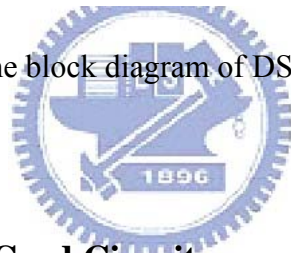


Fig. 3-18: The block diagram of DSP system [77]



3.3.2 The Expanded SD Card Circuit

The expanded SD card circuit was designed to expand the function of DSP module. DSP module and expanded SD card circuit communicated with each other via SPI interface. Here, DSP module was set as Master configuration, and expanded SD card circuit was set as Slave configuration, as shown in Fig. 3-19.

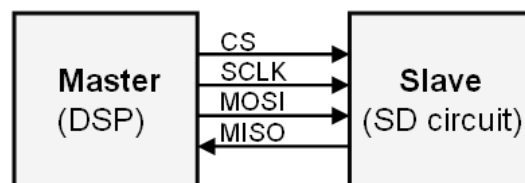


Fig. 3-19: Handshake mode between DSP module and expanded SD card circuit

In this expanded SD card circuit, another microcontroller MSP430F2013 was

used as the core of this circuit. This controller only has 14 pins and its size is 5.1 mm x 6.2 mm. MSP430F2013 can provide many benefits, such as inner 32768 Hz oscillator, two pair I/O ports, USI (Universal Serial Interface) interface, Timer interrupt, watch dog timer, 16-bit Sigma-Delta Analog to Digital converter, etc. The expanded SD card circuit included a microcontroller, an ICE download pin, SD/MMC interface connection, a buzzer, and a LED. The function block diagram was shown in Fig. 3-20. The schematic circuit of expanded SD card circuit was shown in Fig. 3-21.

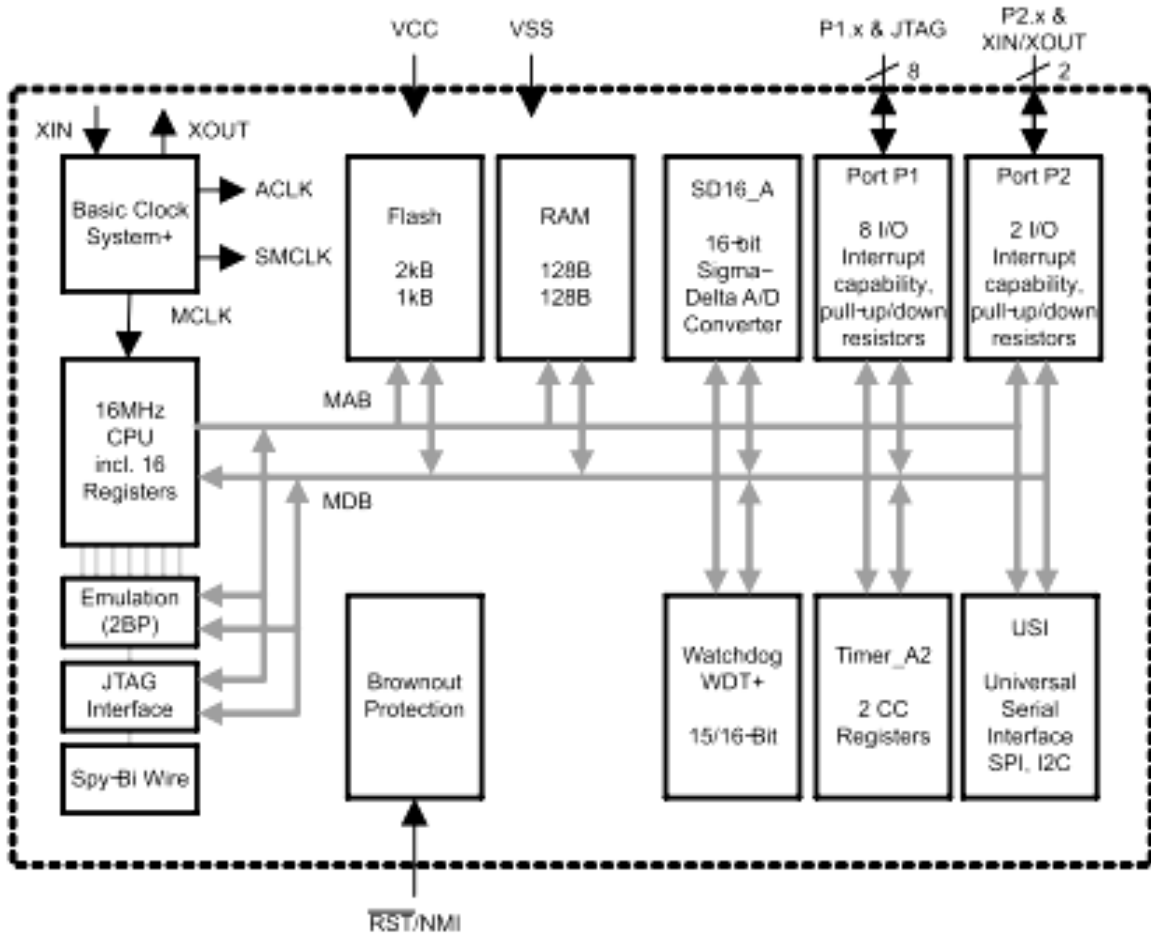


Fig. 3-20: The function block diagram of MSP430F2013

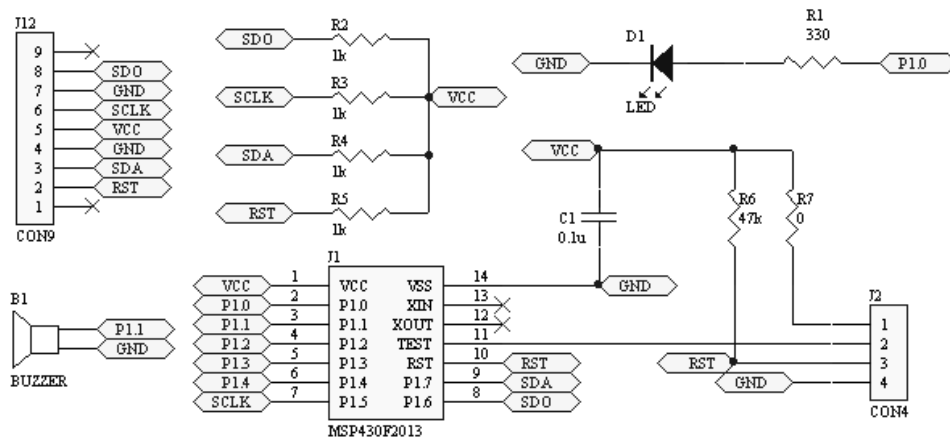


Fig. 3-21: Schematic circuit of expanded SD card circuit

The operating flow chart of expanded SD card circuit was shown in Fig. 3-22. Here, MSP430F2013 in expanded SD card circuit always waited to receive commands from DSP module. When command data was arrived, expanded SD card circuit would start USI interrupt. Second, the command data for expanded SD card circuit was defined as two different warning modes. In mode one, low frequency warning tone would be generated by an interval PWM, and in mode two, high frequency warning tone would be generated by a high potential signal.

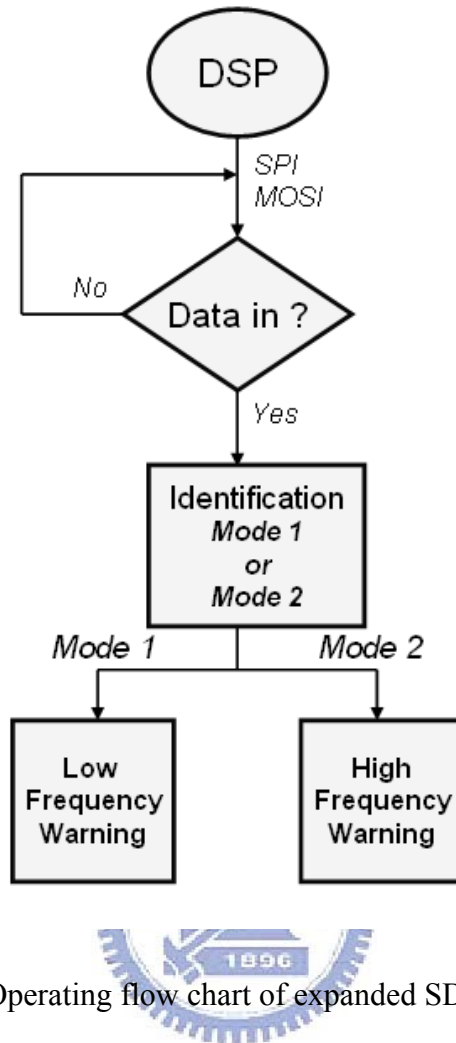


Fig. 3-22: Operating flow chart of expanded SD card circuit

3.4 Hardware System Implementation

A. Portable EEG acquisition module

Fig. 3-23(a ~ c) are the front-end analog circuit and digital control circuit in our portable EEG acquisition module, and the whole EEG acquisition module respectively, and the size of each circuit compared with a coin of one NTD was shown in Fig. 3-23. There are three leads in our portable EEG acquisition module, includes EEG input, reference, and virtual ground of the front-end analog circuit. The electrodes connected with the leads of virtual ground and EEG reference were placed on user's forehead

and behind right ear respectively. The specification of portable EEG acquisition module was listed in Table 3-3.

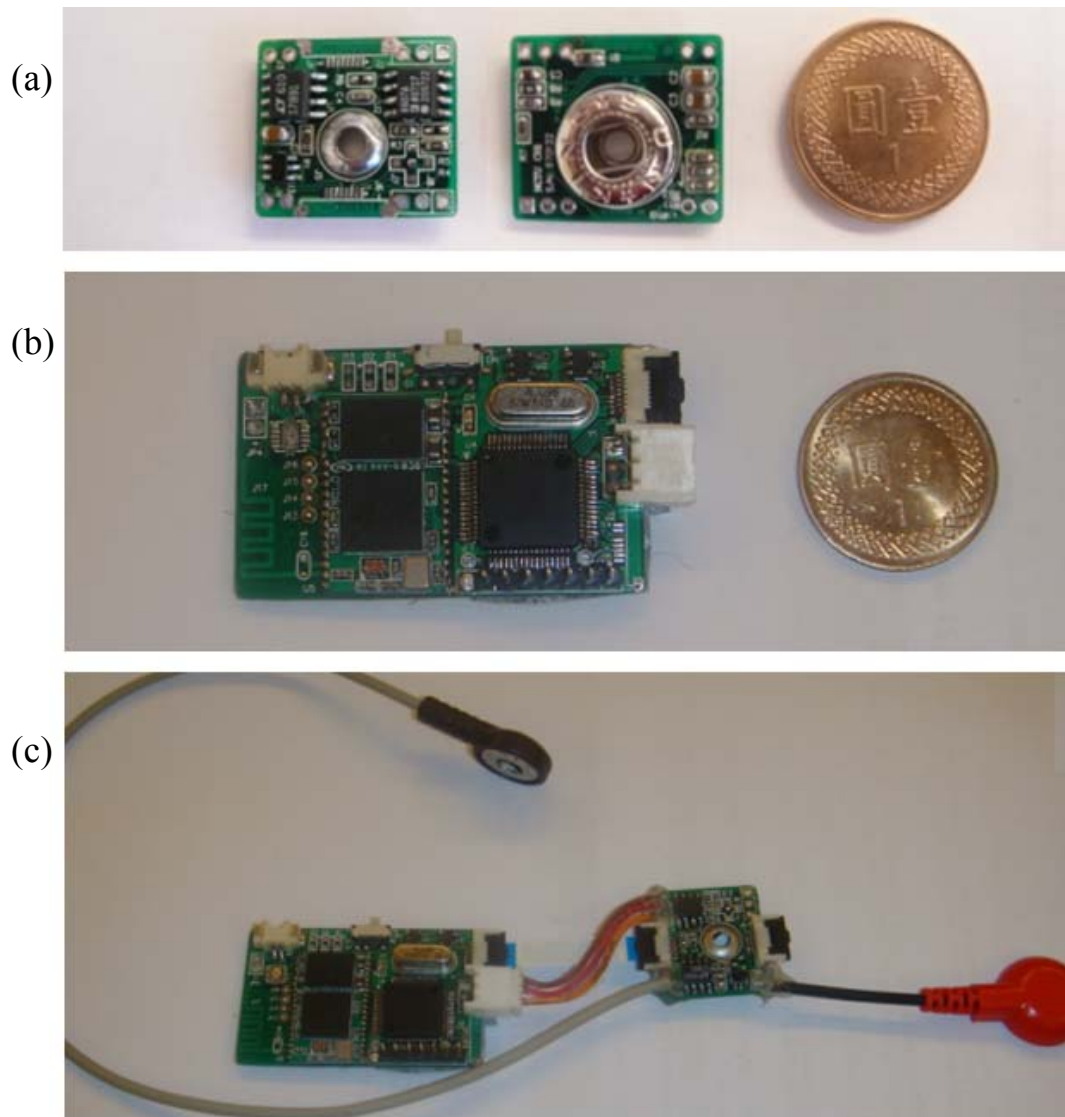
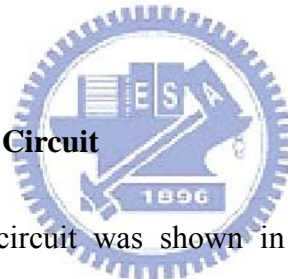


Fig. 3-23: (a) The front-end analog circuit, (b) the digital control circuit, and (c) the whole portable EEG acquisition module with single channel.

Table 3-3: The spec of portable EEG acquisition module

Type	Portable EEG Acquisition Module
Channel Number	1~8
System Output Voltage Range	0~3V
Gain	5000
Bandwidth	0.1~100Hz
ADC Resolution	12bits
Output Current	29.5mA
Battery	Lithium 3.7V 450mAh 15~33hr
Full Scale Input Range	577 μ V
Sampling	512Hz
Input Impedance	greater than 10M Ω
Common Mode Rejection Ratio	77dB
Power Supply Rejection Ratio	88dB
Size	18mm x 20mm and 25mm x 40mm

B. DSP Module and SD Card Circuit



The expanded SD card circuit was shown in Fig. 3-24(a). It looked like a SD/MMC card, which can easily be plugged into the SD/MMC socket in DSP module. The size of expanded SD card circuit is 24mm x 32mm. Fig. 3-24(b) is the illustration for application of expanded SD card circuit.

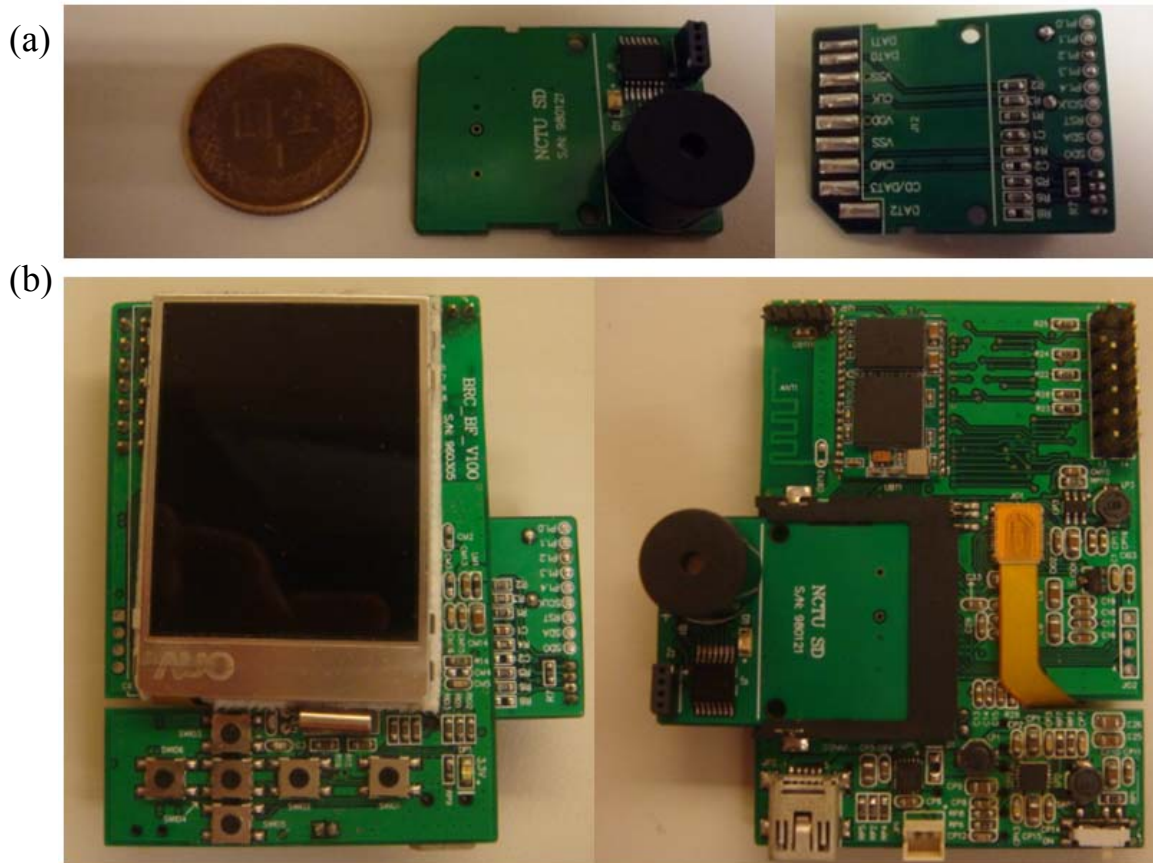
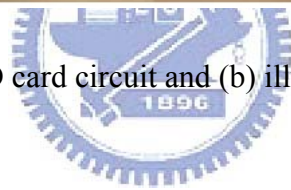


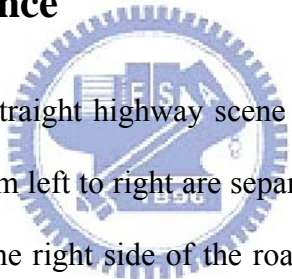
Fig. 3-24: (a) The expanded SD card circuit and (b) illustration for application of expanded SD card circuit



Chapter4 Unsupervised Approach

Based on the unsupervised analysis flowchart in Fig. 2-8, we will further discuss the details of every analysis diagrams in the following sessions. In order to find out the real driving behavior information, first we calculate the driver's driving performance by using the record in simulation experiment. Moreover, we use the unsupervised analysis method to analyze the corresponding EEG information, including the preprocessing, alert model construction, and computation of the deviation using Mahalanobis distance method.

4.1 Driving Performance



The VR-based four-lane straight highway scene was applied in the experiment. In this scene, the four lanes from left to right are separated by a median stripe and the distance from the left side to the right side of the road was equally divided into 256 points indicating the position of the vehicle as the digital output signal of the VR scene at each time instant. The width of each lane and the car is 60 units and 32 units, respectively. Fig. 2-4 shows an example of the driving performance represented by the vehicle deviation trajectories. We have defined an indirect index of the subject's alertness level (driving performance) as the deviation between the center of the vehicle and the center of the cruising lane. VR driving simulation environment will randomly start a deviation event to move the car to right or left side in the car driving experiments. Subjects needs to sense those sudden movements and trying to make a reversely turn to back to the third lane. At one time, the VR environment also outputs the driving events inside the data of car trajectories, as deviation event start trigger, response onset trigger; and response offset trigger. Fig. 4-1 shows the example of

deviation event.

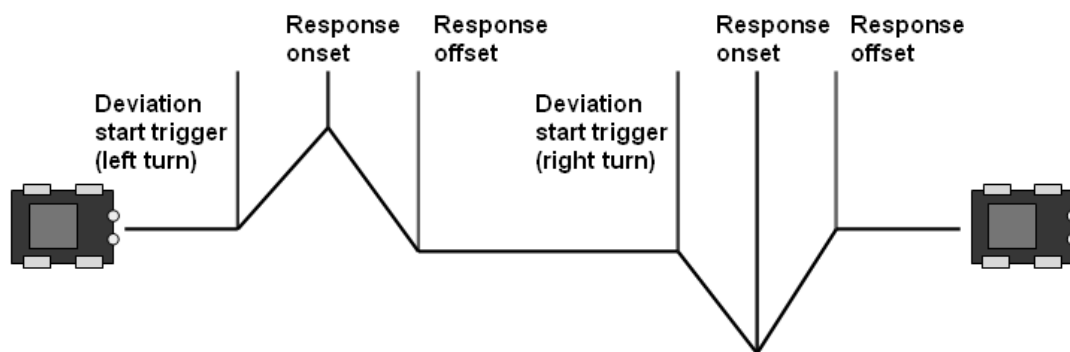


Fig. 4-1: The example of deviation event and car trajectories

In Fig. 4-2, the driving trajectories that we recorded followed below steps to show the driving performance. For restoring trajectories data, event trigger removal is the first process that we do. After deviation response offset, the positions of every experiment trial aren't consistent, so that we need to remove the baseline every trial. The results of the second step will leave right or left turn trajectories. And then absolute trials to collocate total right / left turn data. Typically the drowsiness level fluctuates with cycle lengths longer than 4 minutes [64], [65], and hence we smooth the indirect alertness level index using a causal 90-sec moving window advancing. This helps us to eliminate variance with cycle lengths shorter than 1-2 minutes. We emphasize that this index is used only to validate our approach, and it is not as an input to develop the model for the alert state of the subject.

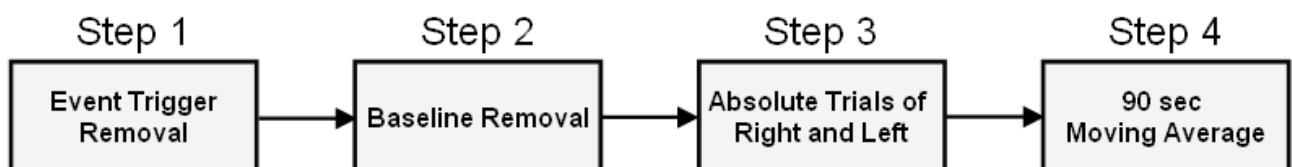


Fig. 4-2: The processing steps of driving performance

Following the above 4 steps, an example of driving performance are shown as

Fig. 4-3. Fig. 4-3(a) shows the original driving data which including event triggers, and Fig. 4-3(b ~ d) shows the results of 4 steps respectively. The final driving performance is in Fig. 4-3(e). Thus, we use this result to compare with MD*(MDT, MDA, and MTC) and implement in correlation analysis with the driver's performance.

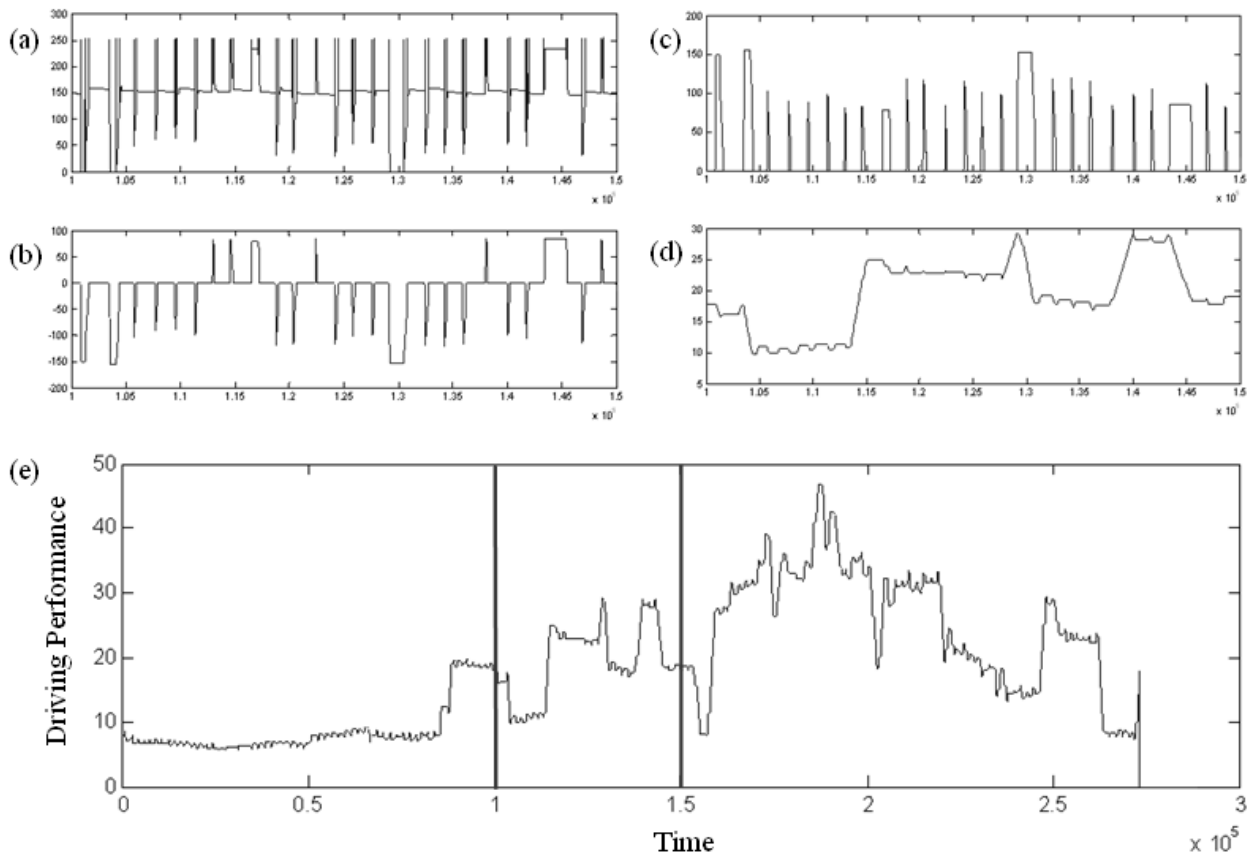


Fig. 4-3: Example of driving performance analysis. (a ~ d) are the fragment of information which marked by two lines. (a) is the original driving trajectories data which including deviation event triggers. (b) is the result which has passed through event trigger removal. (c) is the absolute result. (d) is the result which has smoothed by 90-sec moving average. (e) shows the total driving performance data.

4.2 Smoothing of the Power Spectra

Before extracting the power spectra of alpha and theta rhythms, raw EEG data would be preprocessed to remove power line noise and increase the resolution in the low frequency spectra. In this smoothing method, we used a moving average, as a low-pass filter to cut-off at 32 Hz in and filter noise over 32 Hz. A moving average filter was used to minimize the presence of artifacts in the EEG records of all sub-windows. Next, we down sample 8 times to 64Hz, so that every sub-window only left 64 points in one second. Those two preprocessing methods can decrease the unnecessary noise and increase the low frequency band information in theta and alpha band spectra. Go on, building up an 8 second moving window to save sub-windows, and displace a sub-window in every 1 second. The first FFT result will be produced at 8th seconds; moreover other FFT results will be in every following 1 second. The smoothing method of moving window can reserve the low frequency information of EEG power spectra longer to further analysis. Thus, for each session EEG log power time series at alpha band as well as at theta band with 1 sec time intervals were generated. Fig. 4-4 showed the processes of spectra analysis as precedence.

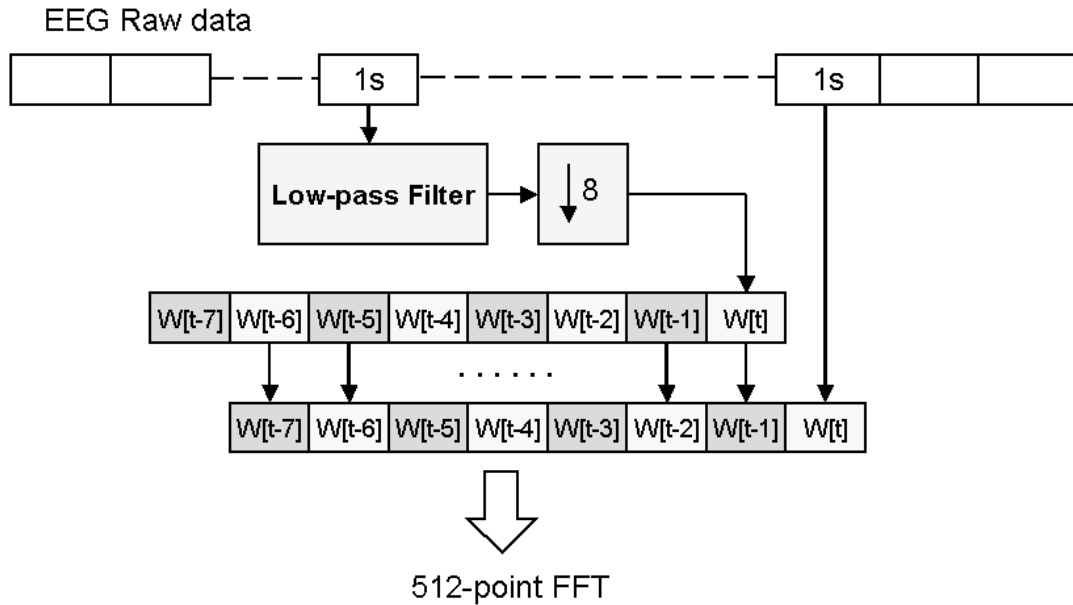


Fig. 4-4: Processes of spectra analysis as precedence

4.3 Construction of the Alertness Model

To investigate the relationship between the measured EEG signals and subject's cognitive state, and to quantify the level of the subject's alertness in our previous studies [78]-[80], first, we need to quantify the volunteer's drowsiness level in this experiment. When subjects fall drowsy, they often exhibit relative inattention to environments, eye closure, less mobility, failure to motor control and making decision. Hence, the vehicle deviations were defined as the subject's drowsiness index.

In our approach for every subject in every driving session a new model will be constructed. Consequently the variability between subjects as well as the inter-session variability is no more important; these are taken into account automatically. To develop the alert model we make a few mild but realistic assumptions as follows:

- (1) The subject is usually very alert immediately after he/she starts the driving session.

- (2) Subject's cognitive state can be characterized by the power spectrum of his/her EEG.
- (3) When the person is in the alert state, it can be modeled reasonably well using a multivariate distribution of the power spectrum.
- (4) The alert model expresses well the EEG spectra when the subject remains alert or return to alert state from drowsiness.

One can argue that the subject may already be in a drowsy state when he/she begins driving. If that is really true, then that can be detected by checking the consistency between two alert models derived using data in two successive time intervals. In other words, we can check whether the two alert-models identifies in two successive time intervals are statistically same or not. If the subject was already in a drowsy state, then he/she will either move to a deep drowsy/sleepy state or will transit to an alert state. In both cases, the two models will not be statistically consistent.

Here we use a multivariate distribution to model the distribution of power spectrum in the alert state. In particular, at every 1 second, we calculate the power spectrum vector in p dimension. In our experiment theta band is located in 32~63 (4~7Hz), and alpha band is in 64~96 (8~12Hz). In this way, a set of $n=60$ data vectors $\{\mathbf{x}_1, \dots, \mathbf{x}_{60}\}$ is generated in every minute. We use 3 minutes of spectral data to derive the alert model. The alert model is represented and characterized by a multivariate normal distribution $N(\mu, \Sigma^2)$, where μ is the mean vector and Σ is the variance-covariance matrix.

We use the maximum likelihood estimates for μ and Σ^2 . After finding the alert model we check whether the EEG spectrum in the alpha band (also in theta band) indeed follows a multivariate normal using Mardia's test [81], [82]. If the model passes the Mardia's test, we accept that model as the alert model. Otherwise, we move

the data window by one minute and again use the next 3 minutes of data to derive and validate the model using Mardia's test. Once a model is built, a significant deviation from the model can be taken as a departure from alertness. Note that, we are saying "departure from alertness" which is not necessarily drowsiness. For example, the subject could be excited over a continued conversation over a mobile phone. In this case, although the person is not drowsy, he/she is not alert as far as the driving task is concerned and hence needs to be cautioned. Thus our approach is more useful than typical drowsiness detection systems. A consistent and significant deviation for some time can be taken as an indicator of drowsiness.

For the sake of completeness, we briefly explain the Mardia's test of multi-variate normality. Given a random sample, $X=\{\mathbf{x}_1, \dots, \mathbf{x}_n\}$ in \mathbb{R}^p , Mardia [81], [82] defined the p-variate skewness and kurtosis as:

$$b_{1,p} = \frac{1}{n^2} \sum_{i=1}^n \sum_{j=1}^n \{(\mathbf{x}_i - \bar{\mathbf{x}})' S^{-1} (\mathbf{x}_j - \bar{\mathbf{x}})\}^3 \quad (4-1)$$

$$b_{2,p} = \frac{1}{n} \sum_{i=1}^n (\mathbf{x}_i - \bar{\mathbf{x}})' S^{-1} (\mathbf{x}_i - \bar{\mathbf{x}})^2 \quad (4-2)$$

In (1) and (2) $\bar{\mathbf{x}}$ and S represent the sample mean vector and covariance matrix, respectively. In this case of university data, $b_{1,p}$ and $b_{2,p}$ reduces to the usual university measures skewness and kurtosis, respectively. If the sample is obtained from a multivariate normal distribution, then the limiting distribution of $b_{1,p}$ is a Chi-square with $p(p+1)(p+2)/6$ degrees of freedom, while that of $\sqrt{n}(b_{2,p} - p(p+2))/8\sqrt{p(p+2)}$ is $N(0,1)$. Hence we can use these statistics to test multi-variate normality. In all our experiments, we have used the routines available for Mardia's test in the R-package [83].

4.4 Computation of the Deviation from the Subject

After the alert model is found, we use it to assess the subject's cognitive state. This was done by finding how the subject's present state, as represented by the EEG power spectra, and was different from the state represented by the alert model. The deviation of the present state from the model is computed using Mahalanobis distance [84] that can account for the covariance between variables while computing the distance. Let the alert model computed using the alpha band be represented by $(\bar{\mathbf{x}}, S)_A$ and that by the theta band be represented by $(\bar{\mathbf{x}}, S)_T$. Let \mathbf{x} be a vector representing the power spectra in the alpha band (or in the theta band) of the EEG of the subject at some time instant, then the deviation of the present state from the model is:

$$MD^*(\mathbf{x}) = \sqrt{(\mathbf{x}-\bar{\mathbf{x}})^T S^{-1} (\mathbf{x}-\bar{\mathbf{x}})} \quad (4-3)$$

In (3) if we use the alpha band model, then * is A, and for the theta band model and data, * will be T. Thus the deviation from the alpha band model will be denoted by MDA and that for the theta band model will be denoted by MDT. Similar to the pre-processing of the indirect alertness level index (driving performance), the MDA/MDT is also smoothed by the moving average method using a window with a window of 90 seconds. The moving average window is shifted by just one value (i.e., 2 sec). For a better visual display, we have scaled the MD* values by subtracting the average MD* computed over the training data used for finding the alert model.

We shall see later that the deviation from either the alpha band model (i.e., MDA) or the theta band model (i.e., MDT) can be used to detect departure from the alert

cognitive state. This raises a natural question, can a combined use of MDA and MDT do a better job than individual ones. To explore such a possibility we use a linear combination MDA and MDT to compute a combined measure of deviation as

$$MDC = a \times MDA + (1-a) \times MDT, 0 \leq a \leq 1. \quad (4-4)$$

4.5 Driving Performance Sorting Analysis

Since the driving performance is an indirect index of the alertness level, we propose the sorted analysis method that sorts the smoothed log power spectra and MD* according to the driving performance index to assess the brain dynamics corresponding to the transition from alertness to drowsiness in driving. This process is used to observe the features change as the increase of driving performance index.

This analysis flow is to separate total trials from the driving trajectories. In our analysis, we assumed that the driving deviation and drowsiness state were direct proportional, so we decided to use the reaction time of driving deviation to be the information of driving performance analysis. Every trial will find out the corresponding EEG raw data. Hence, according to the alertness model in first 3 minutes, the frequency domain spectrum under the deviation can be changed out by FFT, and continually, the MDT and MDA power can also be transformed. Further, the trials are sorted following the length of deviations, and the synchronized MD* power spectra also be sorted together. The width of road was divided into 256 points, and speed of car drifting after deviation onset was 64 points/sec; in other words, the car would drift 1/4 width of road and crash into the second lane or fourth lane in one second. After trials sorting, according to above theory, we can separate the sorting data into 4 segments: alertness (0.2~1s), slight drowsiness (1~2s), extreme drowsiness

(2~3s), and sleepiness (over 3s). Then, the mean and standard deviation in every segment which we counted shows the relationship between driving performance and drowsiness state. The process of sorting analysis is shown as Fig. 4-5. The results of sorting analysis will be discussed in next session.

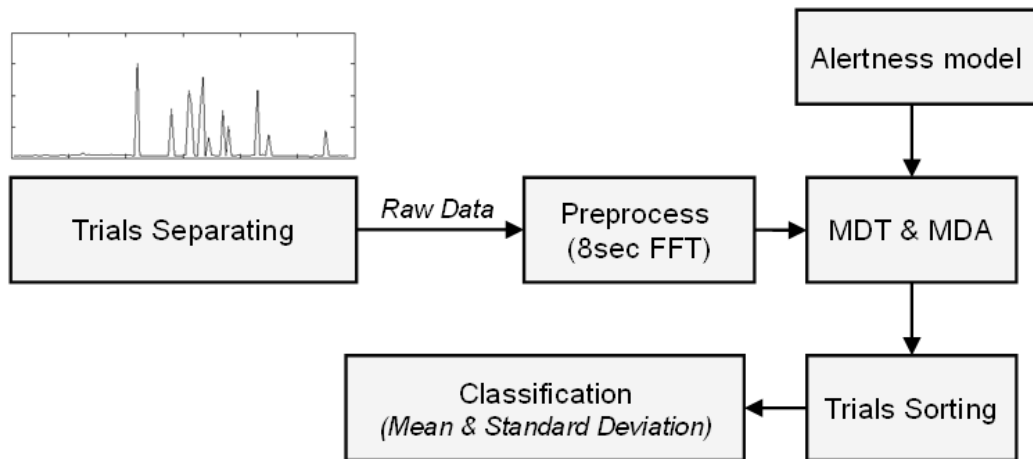


Fig. 4-5: Process of sorting analysis



Chapter5 Results and Discussion

In this chapter, we will separate into two parts to discuss, including the performance of portable EEG acquisition module and the relationship between driving performance and unsupervised analysis. In the first segment, we use sine wave and alpha wave to test the performance correlation. The next segment we will discuss the unsupervised result by using correlation with driving performance, sorting analysis, and linear combination to find out the proportional relationship. And finally we use the binary classification method to summarize the threshold from alertness to drowsiness, furthermore set the optimal threshold into the program of DSP module.

5.1 Performance of Portable EEG Acquisition Module

In this section, the reliability of the proposed portable EEG acquisition module was examined. First, several sine waves with different frequencies generated by a function generator was used as input signal to test whether the EEG acquisition module can stably and validly acquire testing signals. Next, alpha rhythm of EEG generated by closing our eyes and relaxing was used as input signals. We analyzed the real EEG signals obtained by our EEG acquisition module, and checked whether the alpha rhythm of EEG can effectively be extracted.

5.1.1 Test for Sine Wave Signal

In this performance test, we tried to test the correlation between the sine-waves which were recorded actually by portable EEG acquisition module and the sin-waves which were generated by MATLAB function. The EEG signals which were recorded

about 23 sec. The result of correlation between two conditions was shown in Fig. 5-1.

And the correlation of total information could up to 0.9765.

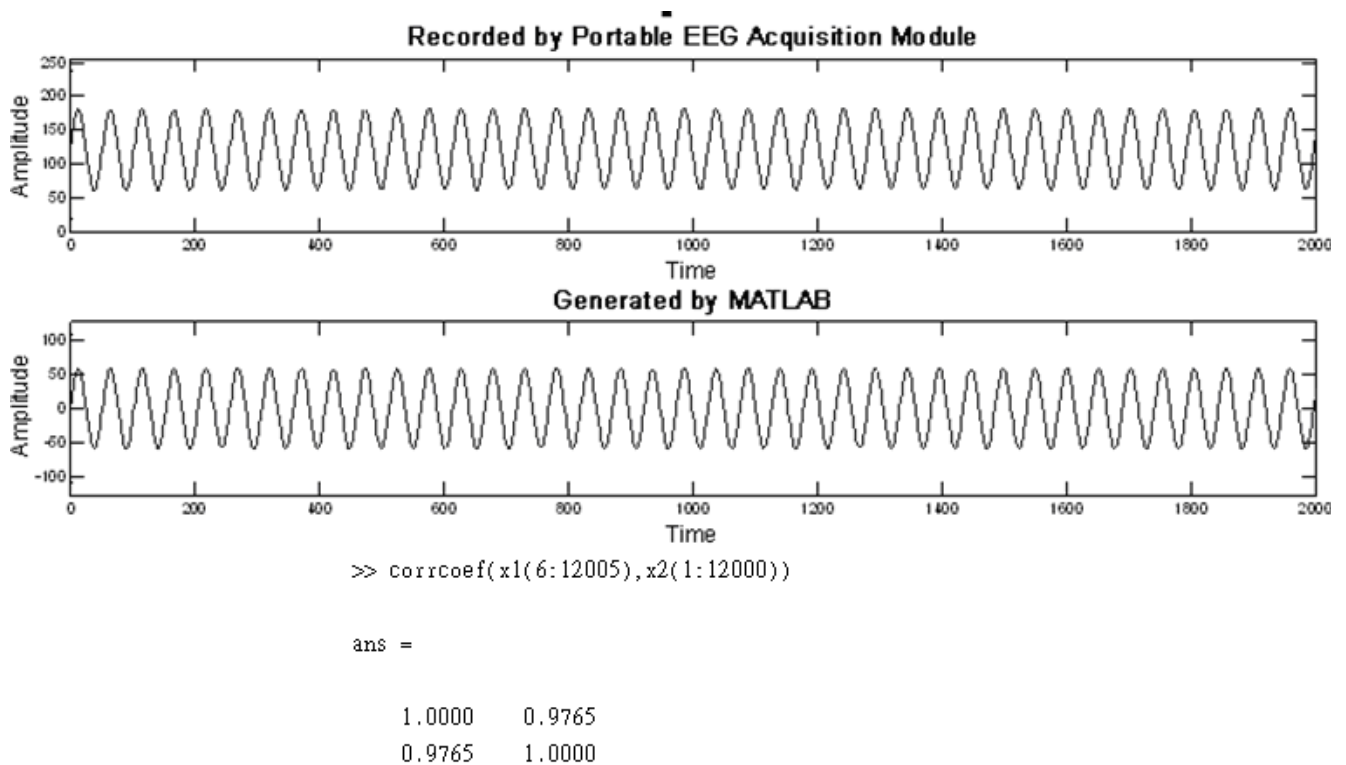


Fig. 5-1: The result of correlation between two conditions

5.1.2 Test for Real EEG Signal

In this system quality test, we recorded a sample EEG data. Subject just open eyes in first 1 second, and start to let eyes close. Subject maintained to stay in relaxed state. In Fig. 5-2, we can notice the alpha wave happened after 1 second, so that we showed time domain and frequency domain information in this figure.

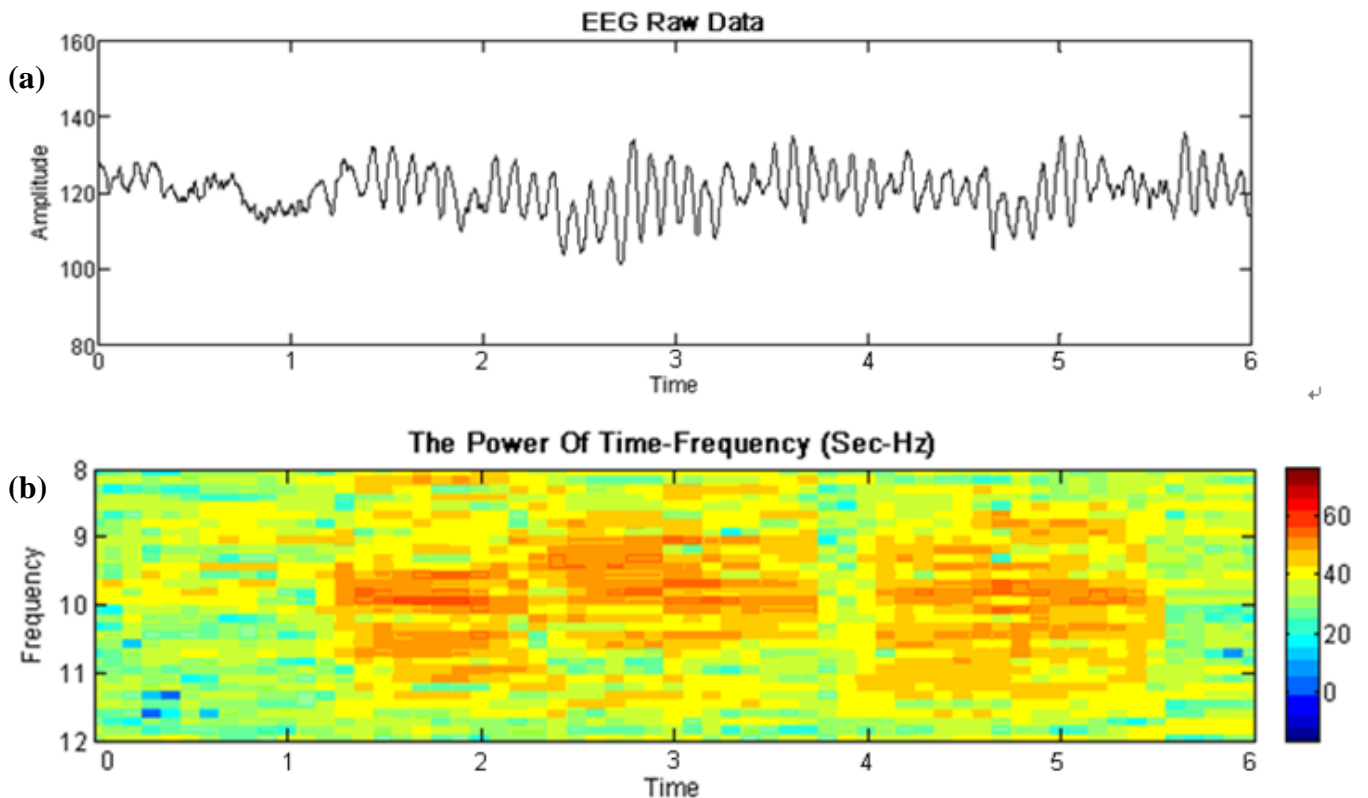
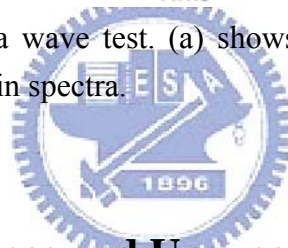


Fig. 5-2: An example of alpha wave test. (a) shows EEG raw data, and (b) is the corresponding frequency domain spectra.



5.2 Driving Performance and Unsupervised Analysis

In this session, we will show the results of algorithm in three parts. First, discuss the relation between driving behavior information and unsupervised analysis in long-term time domain experiments. Second, separating the behavior trials hence finds the corresponding EEG data, then sorting both information checks the connection between MDA / MDT and the reaction time of driving performance. Final, using linear combination finds out MDC and check the highest correlation between both two information.

5.2.1 Results of Unsupervised Analysis

Following the steps of preprocessing and the unsupervised analysis in above chapters, we used OZ channel which has the highest average correlation in 10-20 system [61] to record EEG signal. Then, we constructed $(\bar{\mathbf{x}}, S)_T$ and $(\bar{\mathbf{x}}, S)_A$ in the alert model, which $\bar{\mathbf{x}}$ and S are mean vector and covariance matrix. Moreover, according to the results of FFT counted the MDT and MDA out. There were two examples to show the results of FFT preprocessing, MDA / MDT, and driving performance, as Fig. 5-3 and Fig. 5-4.



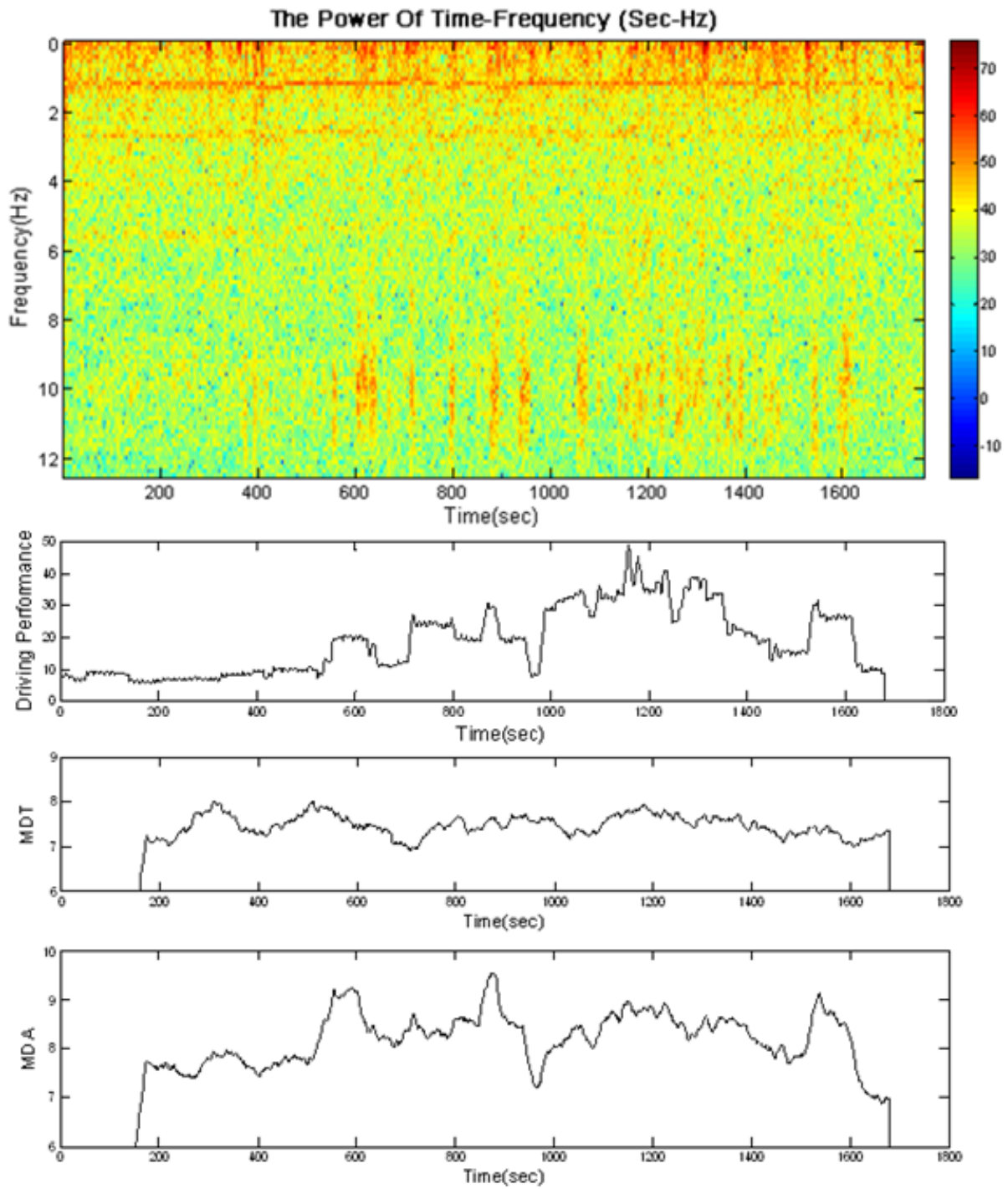


Fig. 5-3: Example 1 of driving performance and unsupervised analysis

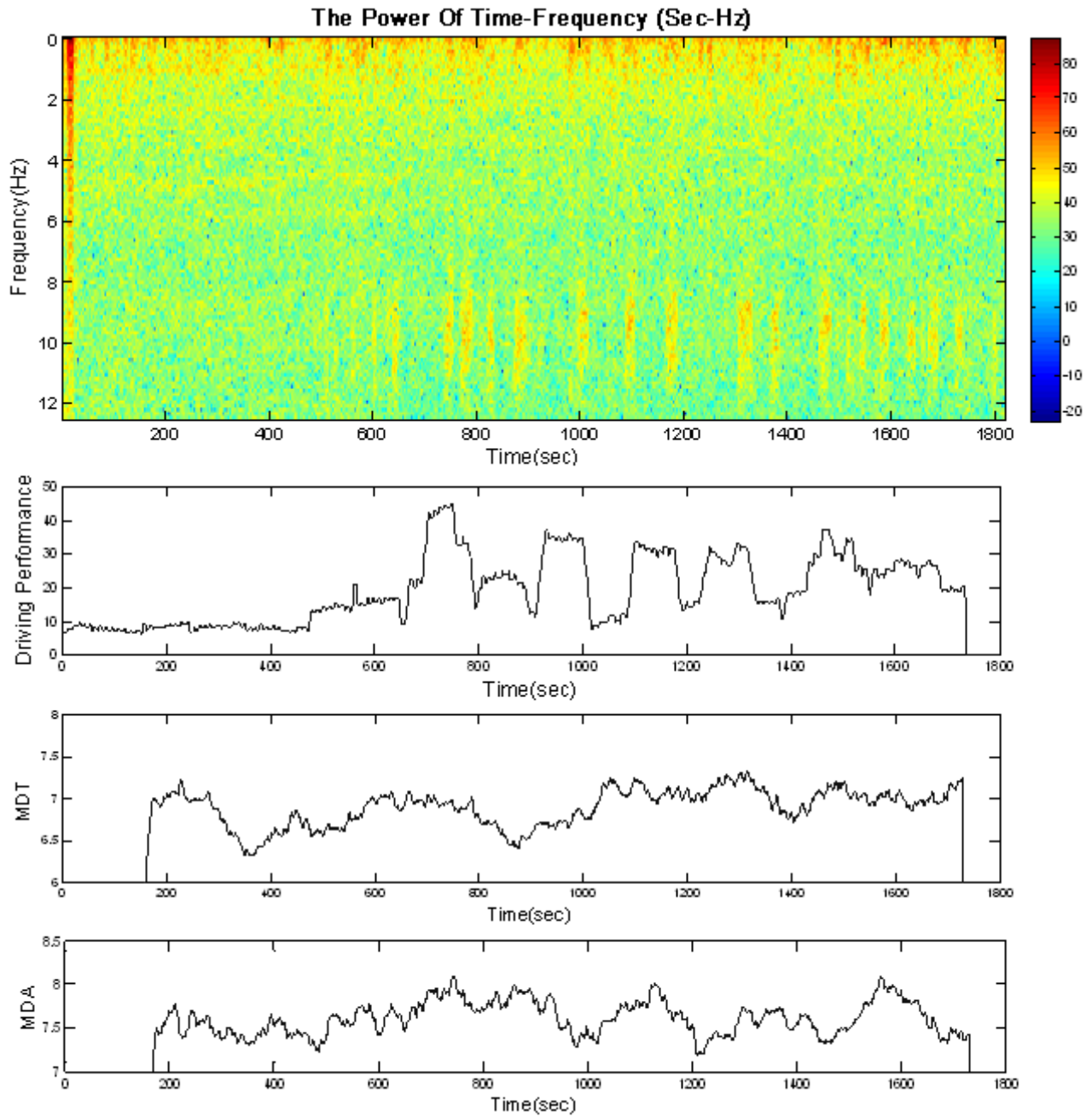


Fig. 5-4: Example 2 of driving performance and unsupervised analysis

From above two cases of unsupervised analysis, we can directly found out the relationship about the variance of frequency domain spectrum and unsupervised analysis when driving performance changed dramatically. According to those experimental results, we can asseverate that EEG waves will be influenced by behavior information when the subjects become drowsiness. And in our portable EEG

acquisition module detects alpha wave clearer and more accurate than theta wave.

5.2.2 Relationship between Driving Performance and Unsupervised Analysis

In reference (N. R. Pal, 2008 [59]) said, they investigated the relationship between the driver's performance and the concurrent changes in the EEG spectrum, and go on, they had sorted the EEG power spectra in alpha band by smoothed driving performance. The similar sorting is also done for power in the theta band. The result which they discovered was that theta and alpha spectrum were directly proportional to the deviation length of driving performance.

Our alert model did not use EEG power directly, but putative MDT and MDA. So next we checked how strongly MDA and MDT were correlated with the driving performance. Fig. 5-5(a) showed the relation between driving performance and MDT (across the 15 test subjects/sessions) while Fig. 5-5(b) exhibited the same for MDA. It was interesting to see that, Fig. 5-5 and the above theory exhibit almost the same behavior; in fact, the average MDT and MDA increased more steadily with driving performance.

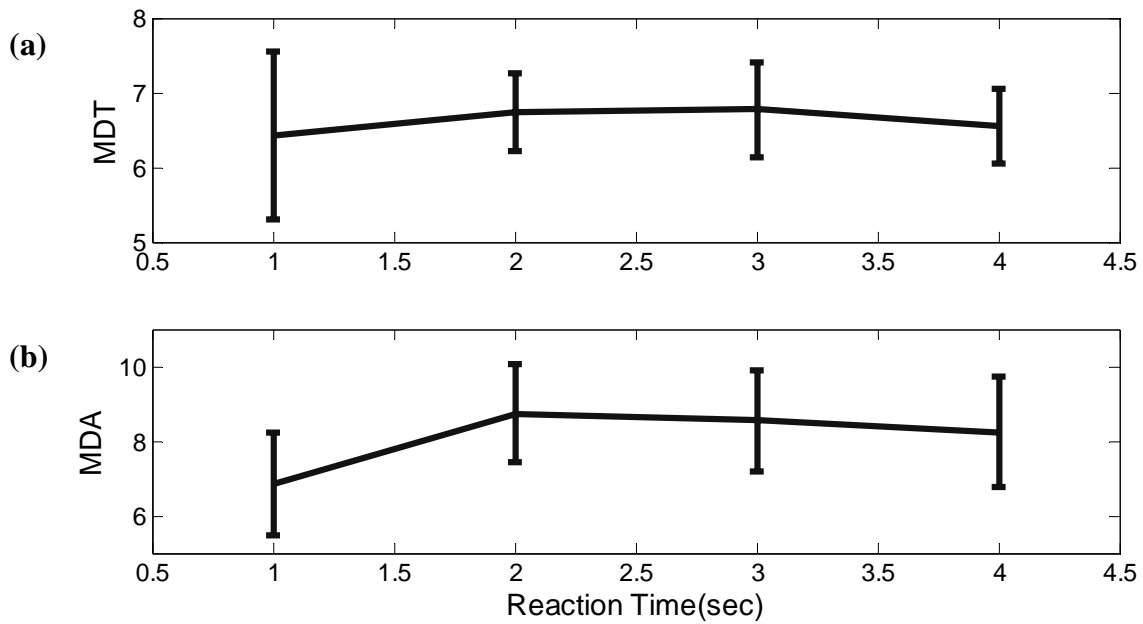


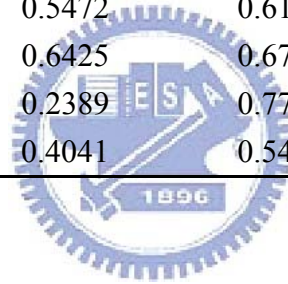
Fig. 5-5: The relationship between MDT / MDA and reaction time

5.2.3 Linear Combination of Model Deviations

To examine this possibility, we consider a very simple linear combination of MDA and MDT as $MDC = a \times MDA + (1-a) \times MDT, 0 \leq a \leq 1$. There are infinitely possible choices for the constant a in the linear combination. We have used a grid search in $a = 0.1, 0.4, 0.6$ and 0.9 and for every such linear combination we have computed the correlation of MDC with driving performance. Table 5-1 lists the correlation values for a few illustrative cases. Note that, in the second column we have two correlation values x/y where x corresponds to MDA (i.e., $a = 1$) and y corresponds to MDT (i.e. $a = 0$). As an example, for subject S1, if we use MDT, the correlation is only 0.6743, while using MDC, for all combinations the correlation is higher than that with MDT. This justifies the utility of the combined model.

Table 5-1: The comparison of the correlation between power and driving performance and MD* and driving performance for channel OZ

Subjects	MDT / MDA	0.1*MDA + 0.9*MDT	0.4*MDA + 0.6*MDT	0.6*MDA + 0.4*MDT	0.9*MDA + 0.1*MDT
S1	0.6743 / 0.7220	0.6818	0.7019	0.7133	0.7278
S2	0.5579 / 0.5607	0.5589	0.5608	0.5613	0.5610
S3	0.4106 / 0.5474	0.4314	0.4714	0.4823	0.5514
S4	0.4737 / 0.5136	0.4791	0.4939	0.5025	0.5168
S5	0.3654 / 0.5469	0.4193	0.5369	0.5643	0.5556
S6	0.1840 / 0.5530	0.2745	0.4866	0.5418	0.5554
S7	0.2520 / 0.6076	0.3827	0.6056	0.6277	0.6143
S8	0.0052 / 0.7942	0.2062	0.6313	0.7342	0.7970
S9	0.2585 / 0.7010	0.2832	0.3832	0.5536	0.6776
S10	0.2004 / 0.4090	0.2022	0.2372	0.3541	0.4144
S11	0.1670 / 0.6020	0.3253	0.5314	0.5725	0.6076
S12	0.3190 / 0.6940	0.3880	0.4602	0.5977	0.6798
S13	0.5186 / 0.5318	0.5472	0.6140	0.6208	0.6224
S14	0.6264 / 0.6713	0.6425	0.6745	0.6820	0.6765
S15	0.1849 / 0.8473	0.2389	0.7708	0.8228	0.8484
Average	0.3465 / 0.6201	0.4041	0.5439	0.5954	0.6271



5.2.4 Threshold Definition and Drowsiness Classification

In drowsiness classification, we use the true-false table to define sensitivity and specificity. Sensitivity and specificity are statistical measures of the performance of a binary classification test. The sensitivity measures the proportion of actual positives which are correctly identified as such (e.g. the percentage of drowsy people who are identified as having the condition); and the specificity measures the proportion of negatives which are correctly identified (e.g. the percentage of alert people who are identified as not having the condition). The relationship between sensitivity and specificity is shown in Fig. 5-6 and the description of binary classification test was in Table 5-2.

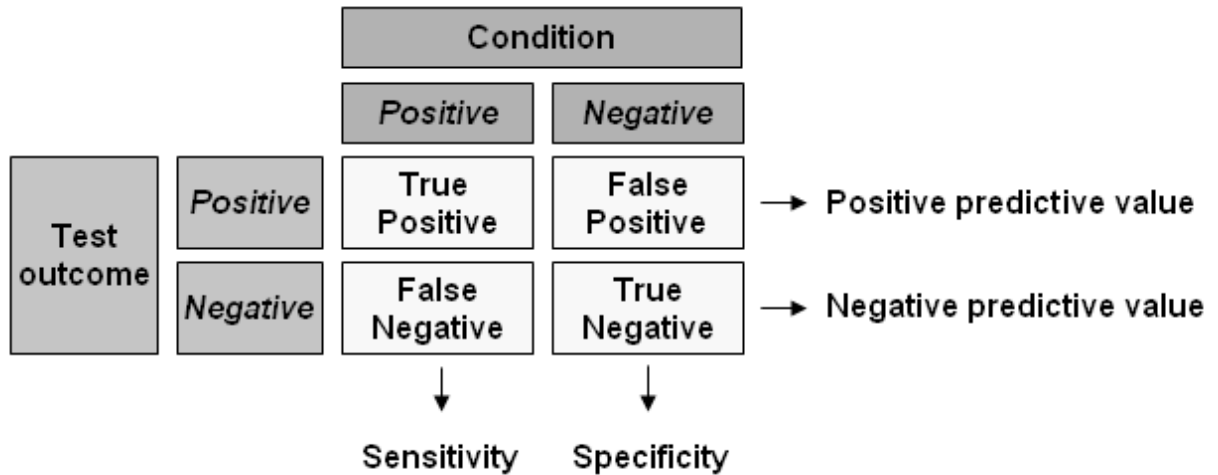


Fig. 5-6: The relationship between sensitivity and specificity

Table 5-2: The description of binary classification test

Type	Description
True positive	Drowsy people correctly diagnosed as drowsy
False positive	Alert people wrongly identified as drowsy
True negative	Alert people correctly identified as alert
False negative	Drowsy Sick people wrongly identified as alert

To define the drowsy state in driving performance and MD*, we need to collect the true positive, false positive, and false negative parameters, hence to analyze the sensitivity and positive predictive value.

A. Positive Predictive Value:

$$PPV = \frac{\text{number of True Positives}}{\text{number of True Positives} + \text{number of False Positives}} \quad (5-1)$$

The positive predictive value, or precision rate, or post-test probability of disease, is the proportion of patients with positive test results who are correctly diagnosed. It is the most important measure of a diagnostic method as it reflects the probability that a

positive test reflects the underlying condition being tested for. Its value does however depend on the prevalence of the disease, which may vary.

B. Sensitivity:

$$\text{Sensitivity} = \frac{\text{number of True Positives}}{\text{number of True Positives} + \text{number of False Negatives}} \quad (5-2)$$

A sensitivity of 100% means that the test recognizes all drowsy people as drowsy. Thus in a high sensitivity test, a negative result is used to rule out the disease. Sensitivity alone does not tell us how well the test predicts other classes (that is, about the negative cases). In the binary classification, as illustrated above, this is the corresponding specificity test, or equivalently, the sensitivity for the other classes. However, sensitivity is not the same as the positive predictive value (ratio of true positives to combined true and false positives), which is as much a statement about the proportion of actual positives in the population being tested as it is about the test.

The calculation of sensitivity does not take into account indeterminate test results. If a test cannot be repeated, the options are to exclude indeterminate samples from analysis (but the number of exclusions should be stated when quoting sensitivity), or, alternatively, indeterminate samples can be treated as false negatives (which gives the worst-case value for sensitivity and may therefore underestimate it).

After explaining the definitions of sensitivity and positive predictive value, the next step is to define the threshold of driving performance and MD*(MDT, MDA, and MDC). The threshold of driving performance can follow above conclusion of sorting analysis which separated into 4 parts: alertness (0.2 ~ 1s), slight drowsiness (1 ~ 2s), extreme drowsiness (2 ~ 3s), and sleepiness (over 3s). Further, we assume that

deviation time is smaller than 1 second to be alert, and others are drowsiness. On the other hand, we need to define the threshold of MD*. Because the results of MD* had been normalized, so we are beneficial to collect all 15 subjects' MD* data and analyze them. In Fig. 5-7 and Fig. 5-8, we set the threshold of MD* from 1 ~ 13 respectively and analyzed the sensitivity and positive predictive value in different threshold. In linear combination, we also tried to separate into 9 conditions: $a = 0.1, 0.2 \dots 0.8, 0.9$. Following the different conditions to find the sensitivity and positive predict value in different threshold of MD*.



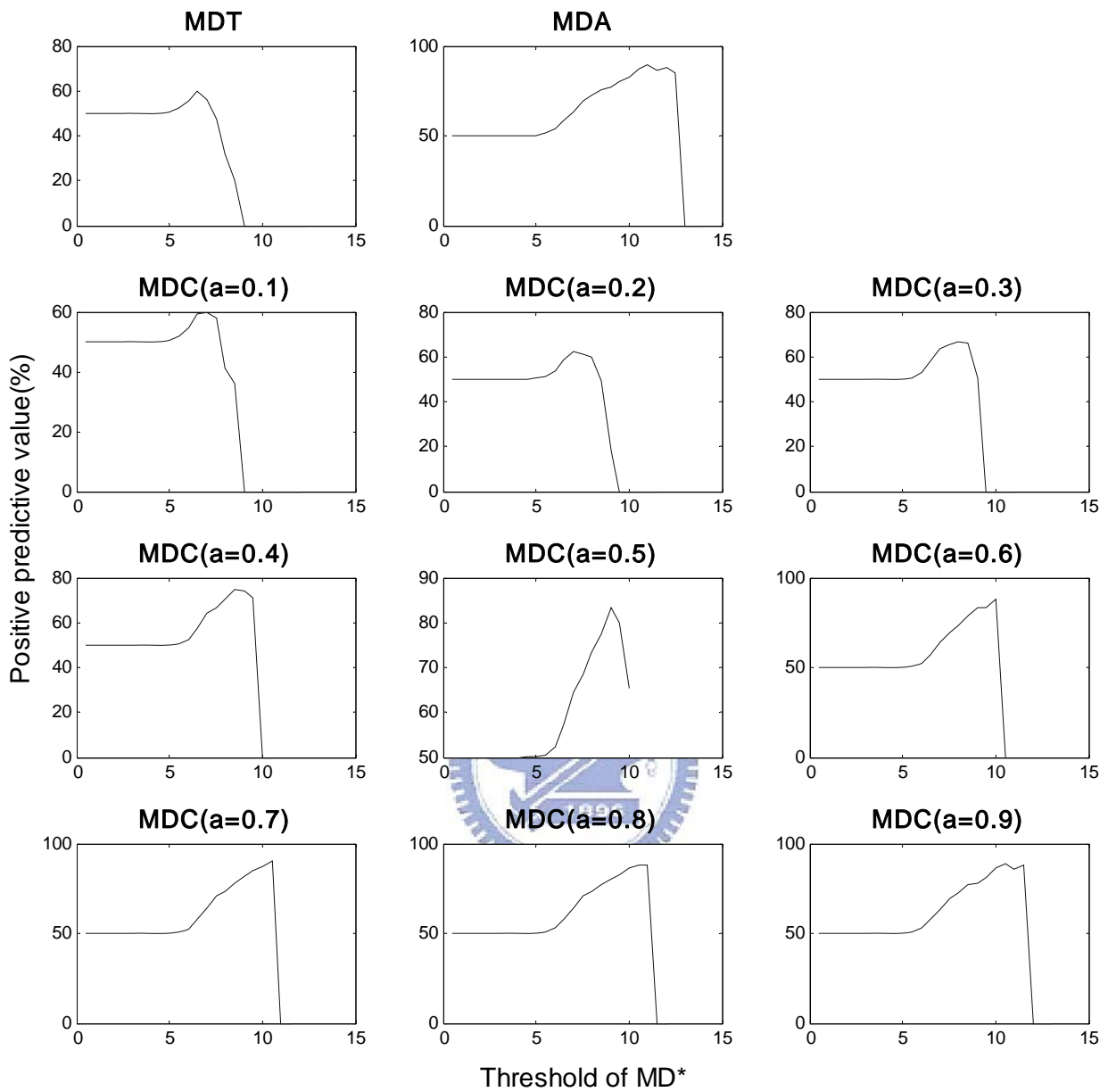


Fig. 5-7: Positive predictive value vs. threshold of MD* (MDT, MTA, and MDC)

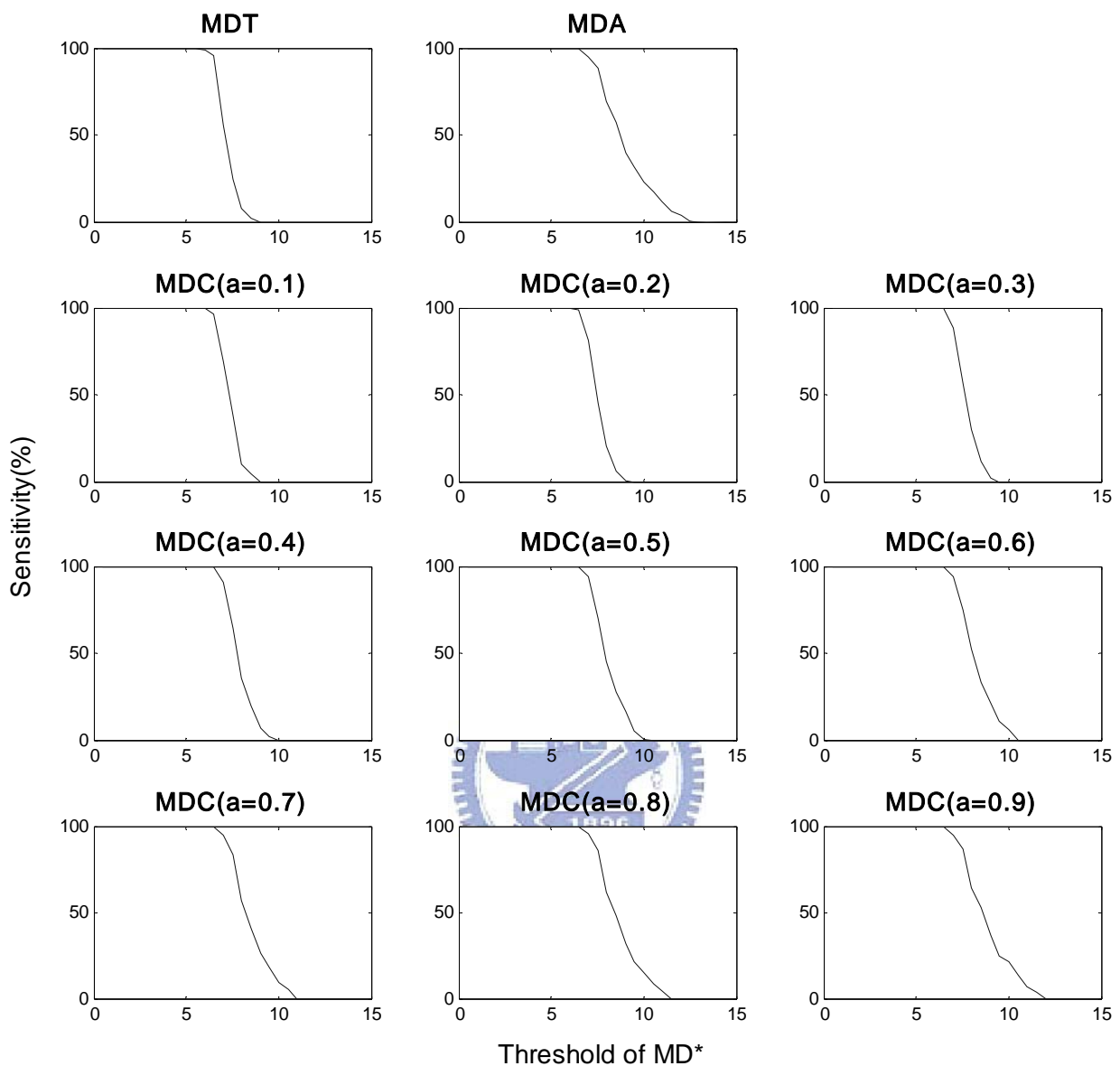


Fig. 5-8: Sensitivity vs. threshold of MD* (MDT, MTA, and MDC)

When finished calculating positive predictive value and sensitivity in different conditions of linear combination, then we needed to choose the suitable threshold of MD*. According to equation 5-3, the F-measure can be used as a single measure of performance of the test. In information retrieval positive predictive value is called

precision, and sensitivity is called recall. The F-measure is the harmonic mean of precision and recall:

$$F - measure = 2 \times \frac{precision \times recall}{precision + recall} \quad (5-3)$$

The results of passing through F-measure were shown as Fig. 5-9. The percent of F-measure mean the ratio of drowsy accuracy actually. Both parameters are associated with drowsiness. In different linear combinational conditions, we could find out the highest result of F-measure in condition a = 0.9. According to this conclusion, this condition composed of the best linear combination of the MDC. Hence, the maximum value of F-measure, 77.59%, happened in the most suitable threshold of MDC, 7.5. So that the corresponding sensitivity was 88.28% and positive predictive value was 69.21%. Those results classified in Table 5-3.

The reason of which F-measure was not high enough was described into 3 critical points:

1. The trials of driving trajectories and corresponding MD* which we picked out didn't use moving average to smooth, because of those sectional EEG information were too short. So that the MD* were not good enough in performance sorting analysis.
2. We found out the relation between driving performance and MD*, hence driving performance and MD* were a sufficient condition but not a necessary condition. When MD* value was high, the corresponding driving performance wasn't high too. There were other variables appending to user's EEG waves.
3. When subjects became drowsy, the MD* will increase, but will not happen immediately. This phenomenon which based on time domain appeared step by

step. So we used trials of driving trajectories to analyze drowsiness was not sufficient to know the exact information of the EEG.

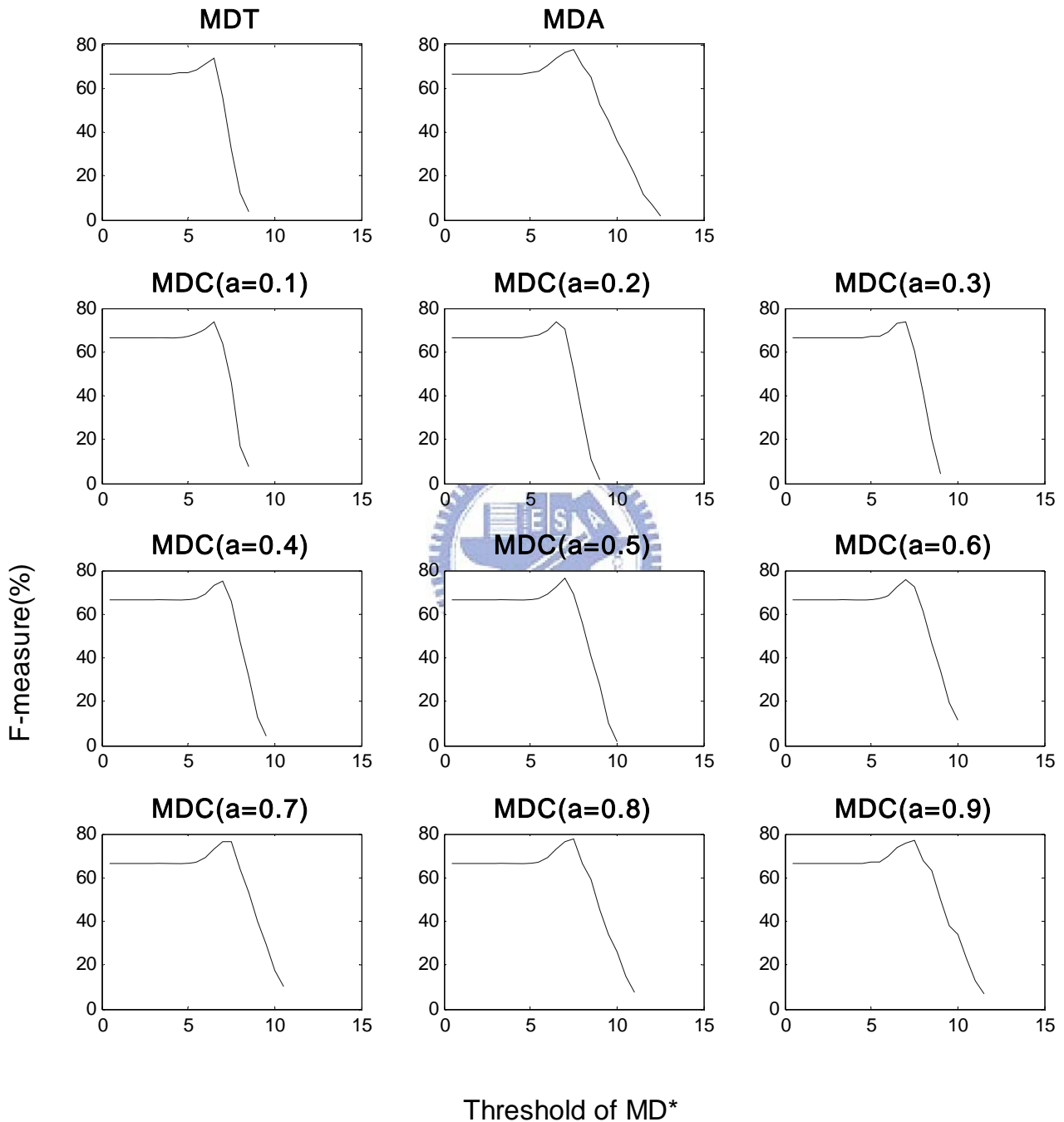


Fig. 5-9: F-measure vs. threshold of MD* (MDT, MTA, and MDC)

Table 5-3: The results of binary classification test

Types	Max F-measure (%)	Corresponding threshold	PPV (%)	Sensitivity (%)
MDT	73.92	6.5	60.15	95.86
MDA	77.34	7.5	69.68	86.90
MDC (a = 0.1)	73.46	6.5	59.29	96.55
MDC (a = 0.2)	73.76	6.5	58.91	98.62
MDC (a = 0.3)	74.02	7	63.73	88.28
MDC (a = 0.4)	75.12	7	63.94	91.03
MDC (a = 0.5)	76.00	7	63.88	93.79
MDC (a = 0.6)	76.28	7	64.28	93.79
MDC (a = 0.7)	76.65	7.5	70.87	83.45
MDC (a = 0.8)	77.40	7.5	70.69	85.52
MDC (a = 0.9)	77.59	7.5	69.21	88.28

5.2.5 DSP Module Programming

The flowchart of DSP module was shown in Fig. 5-10. In program development, we used multithread to build up a real-time analysis system, moreover to increase program's flexibility and the use of performance.

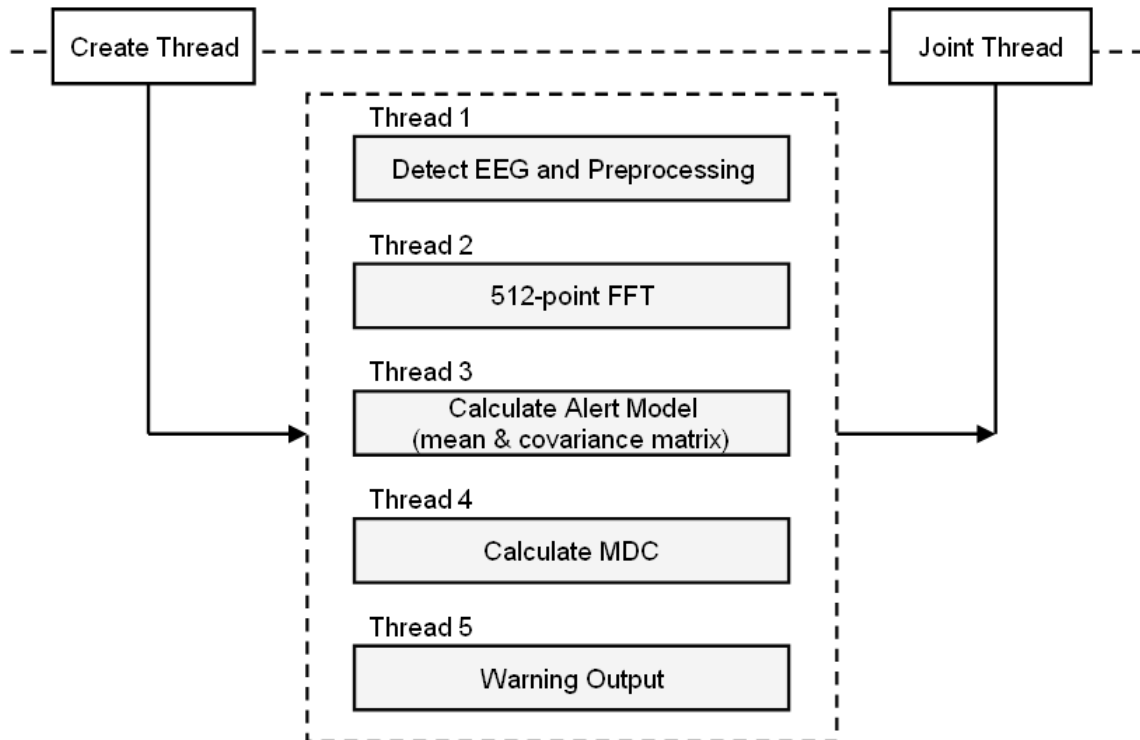


Fig. 5-10: The flowchart of DSP module program

Each thread is independent. In the DSP module's main loop, we just create the threads we want and joint them. The system kernel will automatically schedule those threads and decrease the system waiting cost. In thread 1, Real-time detect EEG raw data from Blue Tooth, and go on pass through a moving average to cut-off at 32Hz, further down sample to 64 point in 1 second. Thread 2 handles FFT process. First, the FFT result will be transmit into 3 minute array in alert model. When array is full, the theta and alpha's mean vector and covariance matrix in thread 3. Thread 4 mainly handles the MDT and MDA converter, then based on above optimal conclusion to calculate the MDC ($a=0.9$). If the values of MDC are higher than threshold in 7.5, the thread 5 will be switch on and make some warning voice in thread 5.

On the other hands, the program's user interface could directly tell user how was his / her physiological conditions. Further, let users easy handle this system. The user interface's flowchart was shown in Fig. 5-11. Following this flowchart, when the boot loader setup, the real-time drowsy detection program will be automatically started by DSP module. If user finished dress the portable EEG acquisition module over, he / she push the start button to start to detect real-time EEG raw data. Then the screen could print the real-time data. Furthermore, according to the mean vector and covariance matrix of alert model, the linear combination of MDT and MDA was counted continually, and the result value will also print on the screen's bottom side. Following Fig. 5-12 showed, the screen's update time we set was changed in every 1 second, so we could show total 1 seconds EEG raw data and result of MDC at the same time on the TFT-LCD, and the expanded SD card circuit will detect a new SPI command from DSP module to ring the buzzer or not in every 1 second. By the way, user could push the quit button to end this program.

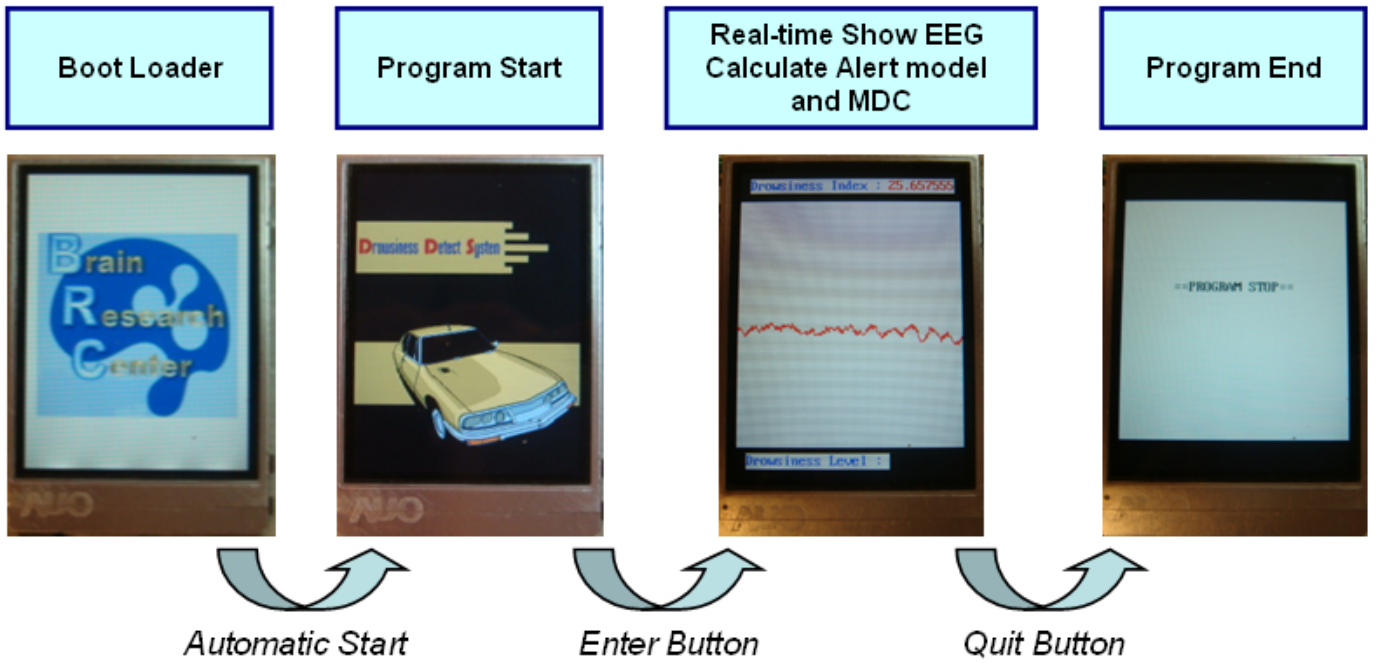


Fig. 5-11: The user interface's flowchart

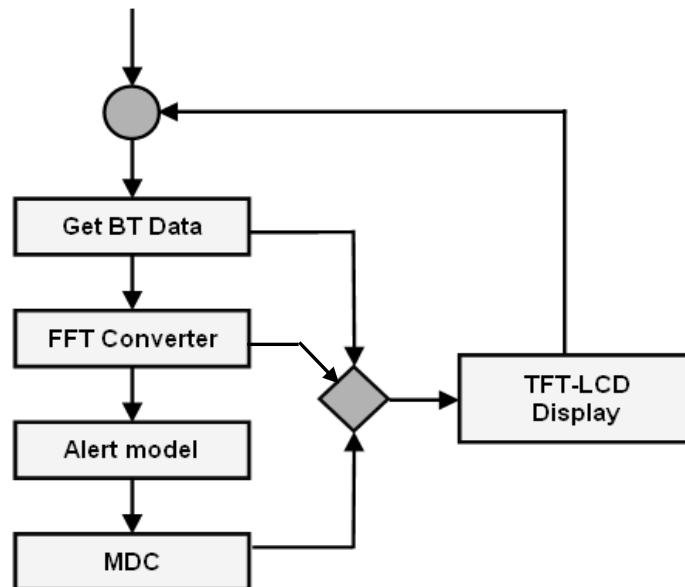


Fig. 5-12: The block diagram of dataflow

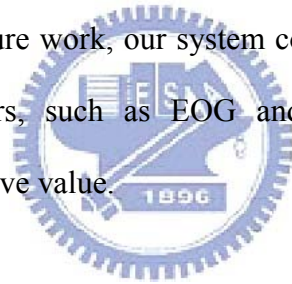
Chapter6 Conclusions

In this study, a real-time wireless brain computer interface for drowsiness detection was proposed. Here, a portable wireless EEG acquisition module and a DSP module were developed. The portable wireless EEG acquisition module was designed to acquire EEG signal, and then transmit them into the DSP module wirelessly to detect drowsiness. The modular approach applied in hardware and software design enables this system to be configurable for different application scenarios. For example, in the future, the EEG acquisition module can be used to connect several optional physiological sensors in addition to the built-in one, and it doesn't affect the whole system architecture. This system is feasible for further extension. Moreover, our EEG acquisition module is small, light, and wearable, therefore, it is suitable for long-term EEG monitoring in users' daily life.

A novel algorithm based on [59] for drowsiness detection was also proposed in this study. It can effectively reduce computation complexity, and is suitable to be implemented in the DSP module, and it is good at removing the differences between individual and environment in different people or measurements. Some previous studies indicated that the level of drowsiness is proportional with the increase of alpha and theta rhythms in EEG. Under the assumption of that driving trajectory is proportional with the level of drowsiness, our experimental results showed that the power of alpha and theta rhythms (the average MDT and MDA) in EEG increased indeed when the level of drowsiness increased, and the linear combination of alpha and theta rhythms (MDC) with factor $a = 0.9$ had the highest correlation (0.6271) with the level of drowsiness.

In this study, the levels of drowsiness were defined as follows: alertness (0.2 - 1s),

slight drowsiness (1 - 2s), extreme drowsiness (2 - 3s), and sleepiness (over 3s). In order to verify the reliability of our proposed algorithm, we simplified four cognitive states into two: alert state and drowsy state (combining slight, deep and extreme drowsiness), and then the binary classification test was used to investigate the sensitivity and positive predictive value of our algorithm with different thresholds. Our experimental results showed that MDC with factor $a = 0.9$ when threshold was set to 7.5 had the highest F-measure value (F-measure = 77.59%, sensitivity = 88.28%, and positive predictive value = 69.21%). However, the accurate of our algorithm for drowsiness detection seems not good enough. This can explained by that each increase of alpha and theta rhythm may not correspond to each drowsy event although the long-term increasing trend of power of alpha and theta rhythm is proportional with the level of drowsiness. In future work, our system could combine with the utility of other physiological parameters, such as EOG and EMG, to improve both the sensitivity and positive predictive value.



References

- [1] Agence France-Presse, Manila, 23rd. [Online]. Available : <http://www.ylps.tp.edu.tw/traffic/news.html>
- [2] K. A. Brookhuis, D. D. Waard, and S. H. Fairclough, "Criteria for driver impairment," *Ergonomics*, Vol 46, 433-445, 2003.
- [3] J. Connor, R. Norton, S. Ameratunga, E. Robinson, I. Civil, R. Dunn, J. Bailey, and R. Jackson, "Driver sleepiness and risk of serious injury to car occupants: population based case control study," *BMJ*, 324: 1125, 2002.
- [4] J. A. Horne, and L. A. Reyner, "Sleep related vehicle accidents," *BMJ*, 310: 565-567 , 1995.
- [5] G. Maycock, "Sleepiness and driving: the experience of UK car drivers," *Journal of Sleep Research*, 5: 229-237, 1996.
- [6] G. Maycock, "Sleepiness and driving: the experience of heavy goods vehicle drivers in the UK," *Journal of Sleep Research*, 6: 238-244, 1997.
- [7] NHTSA, Traffic safety facts 2001: A compilation of motor vehicle crash data from the fatality analysis reporting system and the general estimates system. In: NHTSA's National Center for Statistics and Analysis, Washington, DC, 2002.
- [8] NSF, Sleep facts and stats, National Sleep Foundation, Washington, DC. [Online]. Available: <http://www.sleepfoundation.org/>
- [9] Steven Kotler, "Vision quest," *Wired Magazine*, September 2002.
- [10] S. P. Levine, J. E. Huggins, S. L. BeMent, R. K. Kushwaha, L. A. Schuh, M. M. Rohde, E. A. Passaro, D. A. Ross, K. V. Elisevich, and B. J. Smith, "A Direct

- Brain Interface Based on Event-Related Potentials,” *IEEE Transactions on Rehabilitation Engineering*, vol. 8, pp. 180-185, 2000.
- [11] N. J. Hill, T. N. Lal, M. Schroder, T. Hinterberger, B. Wilhelm, F. Nijboer, U. Mochty, G. Widman, C. Elger, B. Scholkopf, A. Kubler, and N. Birbaumer, “Classifying EEG and ECoG Signals Without Subject Training for Fast BCI Implementation: Comparison of Nonparalyzed and Completely Paralyzed Subjects,” *IEEE Transactions on Neural Systems and Rehabilitation Engineering*, vol. 14, pp. 183-186, 2006.
- [12] J. A. Wilson, E. A. Felton, P. C. Garell, G. Schalk, and J. C. Williams, “ECoG Factors Underlying Multimodal Control of a Brain-Computer Interface,” *IEEE Transactions on Neural Systems and Rehabilitation Engineering*, vol. 14, pp. 246-250, 2006.
- [13] E. C. Leuthardt, K. J. Miller, G. Schalk, R. P. N. Rao, and J. G. Ojemann, “Electrocorticography- based Brain Computer Interface - The Seattle Experience,” *IEEE Transactions on Neural Systems and Rehabilitation Engineering*, vol. 14, pp. 194-198, 2006.
- [14] T. Elbert, B. Rockstroh, W. Lutzenberger, and N. Birbaumer, “Biofeedback of Slow Cortical Potentials,” *Electroencephalography and Clinical Neurophysiology*, vol. 48, pp. 293-301, 1980.
- [15] N. Birbaumer, A. Kubler, N. Ghanayim, T. Hinterberger, J. Perelmouter, J. Kaiser, I. Iversen, B. Kotchoubey, N. Neumann, and H. Flor, “The Thought Translation Device (TTD) for Completely Paralyzed Patients,” *IEEE Transactions on Rehabilitation Engineering*, vol. 8, pp. 190–193, 2000.

- [16] T. Hinterberger, S. Schmidt, N. Neumann, J. Mellinger, B. Blankertz, G. Curio, and N. Birbaumer, "Brain-Computer Communication and Slow Cortical Potentials," *IEEE Transactions on Biomedical Engineering*, vol. 51, pp. 1011-1018, 2004.
- [17] Y. Wang, R. Wang, X. Gao, B. Hong, and S. Gao, "A Practical VEP-Based Brain-Computer Interface," *IEEE Transactions on Neural Systems and Rehabilitation Engineering*, vol. 14, pp. 234-239, 2006.
- [18] E. W. Sellers, A. Kubler, and E. Donchin, "Brain-Computer Interface Research at the University of South Florida Cognitive Psychophysiology Laboratory: The P300 Speller," *IEEE Transactions on Neural Systems and Rehabilitation Engineering*, pp. 221-224, 2006.
- [19] K. D. Nielsen, A. F. Cabrera, and O. F. Nascimento, "EEG Based BCI-Towards a Better Control. Brain-Computer Interface Research at Aalborg University," *IEEE Transactions on Neural Systems and Rehabilitation Engineering*, vol. 14, pp. 202-204, 2006.
- [20] Z. Lin, C. Zhang, W. Wu, and X. Gao, "Frequency Recognition Based on Canonical Correlation Analysis for SSVEP-Based BCIs," *IEEE Transactions on Biomedical Engineering*, vol. 53, pp. 2610-2614, 2006.
- [21] M. Thulasidas, C. Guan, and J. Wu, "Robust Classification of EEG Signal for Brain-Computer Interface," *IEEE Transactions on Neural Systems and Rehabilitation Engineering*, vol. 14, pp. 24-29, 2006.
- [22] G. Dornhege, B. Blankertz, G. Curio, and K. R. Muller, "Boosting Bit Rates in Noninvasive EEG Single-Trial Classifications by Feature Combination and

- Multiclass Paradigms,” *IEEE Transactions on Biomedical Engineering*, vol. 51, pp. 993-1002, 2004.
- [23] T. M. Vaughan, D. J. McFarland, G. Schalk, W. A. Sarnacki, D. J. Krusienski, E. W. Sellers, and J. R. Wolpaw, “The Wadsworth BCI Research and Development Program: At Home With BCI,” *IEEE Transactions on Neural Systems and Rehabilitation Engineering*, vol. 14, pp. 229-233, 2006.
- [24] C. Guger, H. Ramoser, and G. Pfurtscheller, “Real-Time EEG Analysis with Subject-Specific Spatial Patterns for a Brain-Computer Interface (BCI),” *IEEE Transactions on Rehabilitation Engineering*, vol. 8, pp. 447-456, 2000.
- [25] G. Pfurtscheller, C. Neuper, C. Guger, W. Harkam, H. Ramoser, A. Schlogl, B. Obermaier, and M. Pregenzer, “Current Trends in Graz Brain-Computer Interface (BCI) Research,” *IEEE Transactions on Biomedical Engineering*, vol. 8, pp. 216-219, 2000.
- [26] J. A. Pineda, D. S. Silverman, A. Vankov, and J. Hestenes, “Learning to Control Brain Rhythms: Making a Brain-Computer Interface Possible,” *IEEE Transactions on Neural Systems and Rehabilitation Engineering*, vol. 11, pp. 181-184, 2003.
- [27] R. Palaniappan, “Utilizing Gamma Band to Improve Mental Task Based Brain-Computer Interface Design,” *IEEE Transactions on Neural Systems and Rehabilitation Engineering*, vol. 14, pp. 299-303, 2006.
- [28] J. R. Millan, and J. Mourino, “Asynchronous BCI and Local Neural Classifiers: An Overview of the Adaptive Brain Interface Project,” *IEEE Transactions on Neural Systems and Rehabilitation Engineering*, vol. 11, pp. 159-161, 2003.

- [29] E. L. Glassman, "A Wavelet-like Filter based on Neuron Action Potentials for Analysis of Human Scalp Electroencephalographs," *IEEE Transactions on Biomedical Engineering*, vol. 52, pp. 1851-1862, 2005.
- [30] D. J. McFarland and J. R. Wolpaw, "Sensorimotor Rhythm-based Braincomputer Interface (BCI): Feature Selection by Regression Improves Performance," *IEEE Transactions on Neural Systems and Rehabilitation Engineering*, vol. 13, pp. 372-379, 2005.
- [31] C. Neuper, A. Schlogl, and G. Pfurtscheller, "Enhancement of Left-right Sensorimotor EEG Differences during Feedback-regulated Motor Imagery," *Journal of Clinical Neurophysiology*, vol. 16, pp. 373-382, 1999.
- [32] R. Stein, D. Weber, Y. Aoyagi, A. Prochazka, J. Wagenaar, S. Shoham, and R. Normann, "Coding of Position by Simultaneously Recorded Sensory Neurons in the Cat Dorsal Root Ganglion," *The Journal of Physiology*, vol. 560, pp. 883-896, 2004.
- [33] S. Lemm, B. Blankertz, G. Curio, and K. R. Muller, "Spatio-spectral Filters for Improved Classification of Single Trial EEG," *IEEE Transactions on Biomedical Engineering*, vol. 52, pp. 1541-1548, 2005.
- [34] B. Kamousi, Z. Liu, and B. He, "Classification of Motor Imagery Tasks for Brain-computer Interface Applications by Means of Two Equivalent Dipoles Analysis," *Transactions on Neural Systems and Rehabilitation Engineering*, vol. 13, pp. 166-171, 2005.
- [35] L. Qin, L. Ding, and B. He, "Motor Imagery Classification by Means of Source Analysis for Brain Computer Interface Applications," *Journal of Neural Engineering*, vol. 1, pp. 135-141, 2004.

- [36] G. R. Muller-Putz, R. Scherer, C. Neuper, and G. Pfurtscheller, "Steady-State Somatosensory Evoked Potentials: Suitable Brain Signals for Brain-Computer Interfaces," *IEEE Transactions on Neural Systems and Rehabilitation Engineering*, vol. 14, pp. 30-37, 2006.
- [37] C. W. Anderson, E. A. Stolz, and S. Shamsunder, "Multivariate Autoregressive Models for Classification of Spontaneous Electroencephalogram during Mental Tasks," *IEEE Transactions on Biomedical Engineering*, vol. 45, pp. 277-286, 1998.
- [38] T. N. Lal, M. Schroder, T. Hinterberger, J. Weston, M. Bogdan, N. Birbaumer, and B. Scholkopf, "Support Vector Channel Selection in BCI," *IEEE Transactions on Biomedical Engineering*, vol. 51, pp. 1003-1010, 2004.
- [39] B. Graimann, J. E. Huggins, S. P. Levine, and G. Pfurtscheller, "Toward a Direct Brain Interface Based on Human Subdural Recordings and Wavelet-Packet Analysis," *IEEE Transactions on Biomedical Engineering*, vol. 51, pp. 954-962, 2004.
- [40] J. del R. Millan, M. Franze, J. Mourino, F. Cincotti, and F. Babiloni, "Relevant EEG Features for the Classification of Spontaneous Motor-related Tasks," *Biological Cybernetics*, vol. 86, pp. 89-95, 2002.
- [41] R. Palaniappan, R. Paramesran, S. Nishida, and N. Saiwaki, "A New Brain-Computer Interface Design Using Fuzzy ARTMAP," *IEEE Transactions on Neural Systems and Rehabilitation Engineering*, vol. 10, pp. 140-148, 2002.
- [42] F. Cincotti, L. Bianchi, G. Birch, C. Guger, J. Mellinger, R. Scherer, R. N. Schmidt, O.Y. Suarez, and G. Schalk, "BCI Meeting 2005- Workshop on

- Technology: Hardware and Software,” *IEEE Transactions on Neural Systems and Rehabilitation Engineering*, vol. 14, pp. 128-131, 2006.
- [43] J. R. Wolpaw, G. E. Loeb, B. Z. Allison, E. Donchin, O. F. Nascimento, W. J. Heetderks, F. Nijboer, W. G. Shain, and J. N. Turner, “BCI Meeting 2005-Workshop on Signal and Recording Methods,” *IEEE Transactions on Neural Systems and Rehabilitation Engineering*, vol. 14, pp. 138-141.
- [44] S. G. Mason, A. Bashashati, M. Fatourechi, K. F. Navarro, and G. E. Birch, “A comprehensive survey of brain interface technology designs,” *Ann. Biomed. Eng.*, vol. 35, no. 2, pp. 137–169, 2007.
- [45] A. Eskandarian, and A. Mortazavi, “Evaluation of a Smart Algorithm for Commercial Vehicle Driver Drowsiness Detection,” *Intelligent Vehicles Symposium, 2007 IEEE*, vol., no., pp.553-559, 13-15 June 2007.
- [46] M. Suzuki, N. Yamamoto, O. Yamamoto, T. Nakano, and S. Yamamoto, “Measurement of Driver's Consciousness by Image Processing -A Method for Presuming Driver's Drowsiness by Eye-Blinks coping with Individual Differences -,” *Systems, Man and Cybernetics, 2006. SMC '06. IEEE International Conference on*, vol.4, no., pp.2891-2896, 8-11 Oct. 2006.
- [47] F. Wang, and H. Qin, “A FPGA based driver drowsiness detecting system,” *Vehicular Electronics and Safety, 2005. IEEE International Conference on*, vol., no., pp. 358-363, 14-16 Oct. 2005.
- [48] T. Hamada, T. Ito, K. Adachi, T. Nakano, and S. Yamamoto, “Detecting method for drivers' drowsiness applicable to individual features,” *Intelligent Transportation Systems, 2003. Proceedings. 2003 IEEE*, vol.2, no., pp. 1405-1410 vol.2, 12-15 Oct. 2003.

- [49] T. Hong, and H. Qin, "Drivers drowsiness detection in embedded system," *Vehicular Electronics and Safety, 2007. ICVES. IEEE International Conference on* , vol., no., pp.1-5, 13-15 Dec. 2007.
- [50] I. Park, J. H. Ahn, and H. Byun, "Efficient Measurement of Eye Blinking under Various Illumination Conditions for Drowsiness Detection Systems," *Pattern Recognition, 2006. ICPR 2006. 18th International Conference on* , vol.1, no., pp.383-386, 2006.
- [51] M. J. Flores, J. M. Armingol, and A. Escalera, "Real-time drowsiness detection system for an intelligent vehicle," *Intelligent Vehicles Symposium, 2008 IEEE* , vol., no., pp.637-642, 4-6 June 2008.
- [52] H. Su, and G. Zheng, "A Partial Least Squares Regression-Based Fusion Model for Predicting the Trend in Drowsiness," *Systems, Man and Cybernetics, Part A: Systems and Humans, IEEE Transactions on* , vol.38, no.5, pp.1085-1092, Sept. 2008
- [53] T. C. Chieh, Mustafa, M. Marzuki, Hussain, Aini, Hendi, S. Farshad, Majlis, and B. Yeop, "Development of vehicle driver drowsiness detection system using electrooculogram (EOG)," *Computers, Communications, & Signal Processing with Special Track on Biomedical Engineering, 2005. CCSP 2005. 1st International Conference on* , vol., no., pp.165-168, 14-16 Nov. 2005.
- [54] C. T. Lin, R. C. Wu, S. F. Liang, W. H. Chao, Y. J. Chen, and T. P. Jung, "EEG-based drowsiness estimation for safety driving using independent component analysis," *Circuits and Systems I: Regular Papers, IEEE Transactions on* , vol.52, no.12, pp. 2726-2738, Dec. 2005.

- [55] C. T. Lin, S. F. Liang, Y. C. Chen, Y. C. Hsu, and L.W. Ko, "Driver's drowsiness estimation by combining EEG signal analysis and ICA-based fuzzy neural networks," *Circuits and Systems, 2006. ISCAS 2006. Proceedings. 2006 IEEE International Symposium on*, vol., no., pp.4 pp.-2128, 2006.
- [56] H. J. Eoh, M. K. Chung, and S. H. Kim, "Electroencephalographic Study of Drowsiness in Simulated Driving with Sleep Deprivation," *International Journal of Industrial Ergonomics*, Volume 35, Issue 4, pp. 307-320, April 2005.
- [57] L. C. Shi, H. Yu, B. L. Lu, "Semi-supervised clustering for vigilance analysis based on EEG," *Proceedings of 20th International Joint Conference on Neural Networks*. 1518–1523, 2007.
- [58] J. W. Fu, M. Li, and B. L. Lu, "Detecting Drowsiness in Driving Simulation Based on EEG," *Autonomous Systems – Self-Organization, Management, and Control Proceedings of the 8th International Workshop*, Shanghai, China, October 6–7, 2008.
- [59] N. R. Pal, C. Y. Chuang, L. W. Ko, C. F. Chao, T.P. Jung, S. F. Liang, and C. T. Lin, "EEG-Based Subject- and Session-independent Drowsiness Detection: An Unsupervised Approach," *EURASIP Journal on Advances in Signal Processing*, Volume 2008, 11 pages, July, 2008.
- [60] Electroencephalography, from wikipedia, the free encyclopedia, [Online]. Available: <http://en.wikipedia.org/wiki/Electroencephalography>
- [61] 莊玠瑤, "利用虛擬實境模擬系統偵測駕駛員從清醒至打瞌睡過程之腦波變化", 國立交通大學, 碩士論文, 民國九十七年。

- [62] C. T. Lin, R. C. Wu, T. P. Jung, S. F. Liang, and T. Y. Huang, "Estimating alertness level based on EEG spectrum analysis," *EURASIP J. Appl. Signal Process*, vol. no. 19, pp. 3165–3174, Mar. 2005.
- [63] W. Klimesch, "EEG alpha and theta oscillations reflect cognitive and memory performance: a review and analysis," *Brain Research*, vol 29, pp. 169–195, 1999
- [64] S. Makeig and T. P. Jung, "Tonic, phasic, and transient EEG correlates of auditory awareness in drowsiness," *Cognitive Brain Research*, vol. 4, pp. 15-25, 1996.
- [65] S. Makeig, T. P. Jung, and T. J. Sejnowski, "Awareness during drowsiness: dynamics and electrophysiological correlates," *Canadian Journal of Experimental Psychology*, vol., 54, pp.266-273, 2000.
- [66] M. A. Schier, "Changes in EEG alpha power during simulated driving: a demonstration," *International Journal of Psychophysiology*, vol. 37, pp.155-162, 2000.
- [67] S. L. Joutsiniemi, S. Kaski, and T. A. Larsen, "Self-organizing map in recognition of topographic patterns of EEG spectra," *IEEE Transactions on Biomedical engineering*, Vol. 42, no. 11, 1995.
- [68] K. V. Mardia, "Mardia's Test of Multinormality," in *S. Kotz and N.L. Johnson, eds., Encyclopedia of Statistical Sciences*, vol. 5, pp. 217-221, 1985.
- [69] 謝弘義, "具備多功排程功能之無線嵌入式腦機介面系統及其在即時汽車駕駛員疲勞狀態偵測與提醒之應用", 國立交通大學, 碩士論文, 民國九十四年。

- [70] 蔡依伶，“即時獨立成份分析演算法應用於無線嵌入式腦機介面”，國立交通大學，碩士論文，民國九十七年。
- [71] A. K. Whitchurch, B. H. Ashok, R. V. Kumar, and K. Sarukesi, “Wireless system for long term EEG monitoring of Absence Epilepsy,” *Biomedical Applications of Micro- and Nanoengineering*, Vol. 4937, 343, 2002.
- [72] I. Obeid, M. A. L. Nicolelis, and P. D. Wolf, “A low power multichannel analog front end for portable neural signal recordings,” *Journal of Neuroscience Methods*, Volume 133, Issues 1-2, 15 February, Pages 27-32, 2004.
- [73] I. Obeid, J. C. Morizio, K. A. Moxon, M. A. L. Nicolelis, and P. D. Wolf, “Two multichannel integrated circuits for neural recording and signal processing,” *Biomedical Engineering, IEEE Transactions on*, vol.50, no.2, pp.255-258, Feb. 2003
- [74] B. Liu, Y. Zhang, Z. Liu, and C. Yin, “An embedded EEG analyzing system based on μ C/os-II,” *Engineering in Medicine and Biology Society, 2007. EMBS 2007. 29th Annual International Conference of the IEEE*, vol., no., pp.2468-2471, 22-26 Aug. 2007.
- [75] G. S. Chen, C. W. Chen, M. S. Ju, C. C. Lin, and C. C. Lu, “Portable Active Surface Laplacian EEG Sensor for Real-Time Mu Rhythms Detection,” *Engineering in Medicine and Biology Society, 2005. IEEE-EMBS 2005. 27th Annual International Conference of the*, vol., no., pp.5424-5426, 17-18 Jan. 2006.
- [76] P. Cao, S. Jia, X. Wang, and J. Zhou, “Wearable and Wireless Multi-Electrophysiological System,” *Medical Devices and Biosensors*, 2006.

3rd IEEE/EMBS International Summer School on , vol., no., pp.83-85, 4-6 Sept. 2006.

- [77] 賴家達，“無線嵌入式生醫平台”，國立交通大學，碩士論文，民國九十七年。
- [78] S. Makeig and T. P. Jung, “Changes in alertness are a principal component of variance in the EEG spectrum,” *NeuroReport*, vol. 7, pp. 213-216, 1995.
- [79] T. P. Jung, S. Makeig, M. Stensmo, and T. J. Sejnowski, “Estimating alertness from the EEG power spectrum,” *IEEE Trans. Biomed. Eng.*, vol. 44, no. 1, pp. 60–69, Jan. 1997.
- [80] S. Makeig and M. Inlow, “Lapses in alertness: Coherence of fluctuations in performance and EEG spectrum,” *Electroencephalography. Clin. Neurophysiol.*, vol. 86, pp. 23–35, 1993.
- [81] K. V. Mardia. “Applications of some measures of multivariate skewness and kurtosis in testing normality and robustness studies,” *Sankhyā, Ser B*, vol. 36, no. 2, pp. 115-128, 1974.
- [82] K. V. Mardia. “Tests of univariate and multivariate normality,” *In: S. Kotz et al., editors, Handbook of Statistics*, vol. 1, pp. 279-320, 1980.
- [83] The R project for statistical computing, [Online]. Available: <http://www.r-project.org/>
- [84] P. C. Mahalanobis, “generalised distance in statistics,” *Proceedings of the National Institute of Science of India* pp. 49 The R Project for Statistical Computing -55, 1936.